NTIA Report 93-299

Comparison of Wideband Propagation in the 902-928 and 1850-1990 MHz Bands in Various Macrocellular Environments

Jeffery A. Wepman
J. Randy Hoffman
Lynette H. Loew
Vincent S. Lawrence

U.S. DEPARTMENT OF COMMERCE
Ronald H. Brown, Secretary

Larry Irving, Assistant Secretary
for Communications and Information

September 1993

CONTENTS

Page

FIGURES iv

TABLES vi

ABSTRACT 1

1. INTRODUCTION 1

2. MEASUREMENT STRATEGY 3

3. MEASUREMENT SYSTEM 4

   3.1 Transmitter 4
   3.2 Receiver 4
   3.3 Differential GPS System and Dead-Reckoning Sensors 4

4. MEASUREMENT PROCEDURE 6

   4.1 Calibration 6
   4.2 Measurement System Setup, Verification, and Data Collection Process 9

5. MEASUREMENT LOCATIONS 11

6. DATA ANALYSIS METHODS AND RESULTS 16

   6.1 RMS Delay Spread 19
   6.2 Multipath Statistics 29
   6.3 Correlation Bandwidth 38

7. SUMMARY AND CONCLUSIONS 47

8. REFERENCES 49

9. ACKNOWLEDGEMENTS 50

FIGURES

Page

Figure 3.1 Photograph of the impulse response measurement van 5

Figure 4.1 Example calibration power delay profile for the 1850-1990 MHz band 7

Figure 5.1 Measurement routes in the urban high-rise cell 12

Figure 5.2 Measurement routes in the urban cell 13

Figure 5.3 Measurement routes in the suburban cell 14

Figure 5.4 Measurement routes in the semi-rural cell 15

Figure 6.1 Probability density (a-b) and cumulative distribution (c) of RMS delay spread for the semi-rural cell using vertically polarized transmit antennas 20

Figure 6.2 Probability density (a-b) and cumulative distribution (c) of RMS delay spread for the suburban cell using vertically polarized transmit antennas 21

Figure 6.3 Probability density (a-b) and cumulative distribution (c) of RMS delay spread for the urban cell using vertically polarized transmit antennas 22

Figure 6.4 Probability density (a-b) and cumulative distribution (c) of RMS delay spread for the urban high-rise cell using vertically polarized transmit antennas 23

Figure 6.5 Probability density (a-b) and cumulative distribution (c) of RMS delay spread for the suburban cell using circularly polarized transmit antennas 25

Figure 6.6 Probability density (a-b) and cumulative distribution (c) of RMS delay spread for the urban high-rise cell using circularly polarized transmit antennas 26

Figure 6.7 Multipath statistics for the semi-rural cell using vertically polarized transmit antennas 31

FIGURES (cont'd)

Figure 6.8 Multipath statistics for the suburban cell using vertically polarized transmit antennas 32

Figure 6.9 Multipath statistics for the urban cell using vertically polarized transmit antennas 33

Figure 6.10 Multipath statistics for the urban high-rise cell using vertically polarized transmit antennas 34

Figure 6.11 Multipath statistics for the suburban cell using circularly polarized transmit antennas 35

Figure 6.12 Multipath statistics for the urban high-rise cell using circularly polarized transmit antennas 36

Figure 6.13 Probability density (a-d) and cumulative distribution (e-f) of correlation bandwidth for the semi-rural cell using vertically polarized transmit antennas 39

Figure 6.14 Probability density (a-d) and cumulative distribution (e-f) of correlation bandwidth for the suburban cell using vertically polarized transmit antennas 40

Figure 6.15 Probability density (a-d) and cumulative distribution (e-f) of correlation bandwidth for the urban cell using vertically polarized transmit antennas 41

Figure 6.16 Probability density (a-d) and cumulative distribution (e-f) of correlation bandwidth for the urban high-rise cell using vertically polarized transmit antennas 42

Figure 6.17 Probability density (a-d) and cumulative distribution (e-f) of correlation bandwidth for the suburban cell using circularly polarized transmit antennas 44

Figure 6.18 Probability density (a-d) and cumulative distribution (e-f) of correlation bandwidth for the urban high-rise cell using circularly polarized transmit antennas 45

TABLES

Page

Table 4.1 Correlation Between Receiver RF Input Power and Total Power in the PDP....8

Table 6.1 Data Sets for Computation of Statistics....16

Table 6.2 Error Bounds on the Sample Cumulative Distributions....18

Table 6.3 Comparison of RMS Delay Spread Values Exceeded in (μs) for 1920 MHz....28

Table 6.4 Comparison of RMS Delay Spread Values Exceeded in (μs) for 915 MHz....28

Table 6.5 Comparison of 50% Correlation Bandwidth Values Not Exceeded (in MHz) for 1920 MHz....46

Table 6.6 Comparison of 50% Correlation Bandwidth Values Not Exceeded (in MHz) for 915 MHz....46

COMPARISON OF WIDEBAND PROPAGATION IN THE 902-928 AND 1850-1990 MHz BANDS IN VARIOUS MACROCELLULAR ENVIRONMENTS

Jeffery A. Wepman, J. Randy Hoffman, Lynette H. Loew, and Vincent S. Lawrence[*]

Impulse response measurements were taken simultaneously in both the 902-928 and 1850-1990 MHz bands using a wideband measurement system consisting of a fixed transmitter and a mobile receiver. Four different macrocells representing typical semi-rural, suburban, urban, and urban high-rise environments were used for the measurements. Vertically polarized transmit and receive antennas were used for all cell; circularly polarized transmit antennas were also used in the suburban and urban high-rise cells. RMS delay spread, correlation bandwidth, and various other multipath power statistics were used to characterize the wideband propagation and to provide a comparison between the two frequency bands, the two transmit antenna polarizations, and the different cell environments. Major differences were not seen in the propagation behavior between the two frequency bands. The urban high-rise cell exhibited the most multipath, showing more delayed signals having higher power and longer delays than in the other cells. An improvement in propagation (less multipath) was seen when using the circularly polarized transmit antennas instead of the vertically polarized ones for 1920 MHz.

Key words: *coherence bandwidth, correlation bandwidth, impulse response measurements, PCS, Personal Communication Services; power delay profiles; RMS delay spread; wideband measurements*

1. INTRODUCTION

A Personal Communication Services (PCS) propagation experiment was conducted to measure impulse responses in the 902-928 and 1850-1990 MHz bands simultaneously.[**] These measurements were taken in four different macrocells (with radii on the order of 3 to 11 km) in the Philadelphia, PA area. The cells were chosen to represent typical semi-rural, suburban, urban, and urban high-rise environments. Measurements were taken in all four cells using

[*] The authors are with the Institute for Telecommunication Sciences, National Telecommunications and Information Administration, U.S. Department of Commerce, Boulder, CO 80303

[**] This effort was sponsored by Bell Atlantic Mobile, Inc.

vertically polarized transmit and receive antennas. In the suburban and urban high-rise cells, measurements were also taken using circularly polarized transmit antennas (the receive antennas were vertically polarized). The impulse response data were analyzed to provide RMS delay spread, correlation bandwidth, and various other multipath power statistics. The results of this data analysis provided a comparison of wideband propagation between the two frequency bands, the two transmit antenna polarizations, and between the different cell types.

Section 2 of this report discusses the measurement strategy. In Section 3, a description of the measurement system is given. The measurement procedure is presented in Section 4. In this section the various calibration methods utilized are discussed in addition to system verification checks and the typical steps taken to perform the measurements within each cell. Section 5 describes the measurement locations. Maps showing the measurement routes are presented along with descriptions of the various cell environments. The data analysis methods and results are presented in the next section. Section 6.1 discusses RMS delay spread. Probability density and cumulative distribution of RMS delay spread are shown for all cell types, both frequencies, and both transmit antenna polarizations. In Section 6.2, the methods used to compute multipath statistics are detailed. The multipath statistics are presented and include computations of the average, standard deviation, and peak received signal power detected at each delay within each cell. In addition, approximations to the cumulative distribution of received signal power at each delay are given. Correlation bandwidth analyses are covered in Section 6.3. The probability density and cumulative distribution of correlation bandwidth are used to compare propagation effects between the different cells, frequencies, and transmit antenna polarizations. Section 7 provides an overall summary and gives some important conclusions.

2. MEASUREMENT STRATEGY

The impulse response measurement system consisted of a transmitter placed at existing cellular base station sites and a receiver located in a measurement van. The measurement system will be further described in Section 3 of this report. Impulse response data were recorded as the measurement van travelled along predetermined routes within each cell. The routes were chosen to provide a representative characterization of the propagation behavior in each cell. Three different acquisition schemes were used to take the data. In all of these schemes, the data were taken simultaneously in both the 902-928 and 1850-1990 MHz bands. In the first scheme, termed fast acquisition, a rapid succession of three impulse responses was taken every 0.5 s. Within this succession of impulses, a time interval of 1.5 ms was used between the beginning of one impulse and the beginning of the next. The data collected using fast acquisition ensures that the Doppler shift can be determined; an important factor for analyses such as angle-of-arrival. Data taken by the second scheme provided a rapid succession of ten impulse responses every 2 s. As in the fast acquisition scheme, within this succession of impulses, a time interval of 1.5 ms was used between the beginning of one impulse and the beginning of the next. In the third acquisition scheme (termed slow acquisition), a succession of ten impulse responses was taken every 1.5 s with a 0.1 s time interval between the impulses. Vehicle velocity was limited to 50 mph or less for the first and second data acquisition schemes. The velocity varied depending on the particular measurement route. For the third acquisition scheme, the vehicle velocity was held constant at approximately 5 mph. The second acquisition scheme was used for only one short run in one of the cells. The other acquisition schemes were used for all of the cells. Although allowing more impulse responses to be averaged, the second acquisition scheme accumulated too much data to manage efficiently and therefore was used sparingly. The data analysis presented in this report used only the data taken with the fast acquisition scheme. Data acquired in this manner was taken over the largest geographical area in each cell and therefore is most representative of the propagation behavior in the entire cell.

A differential Global Positioning System (GPS) receiver and dead-reckoning system were employed to store time and vehicle position information for the measurement van in a separate file as impulse response data were recorded. The impulse response data were time-stamped to allow correlation between the impulse responses and measurement vehicle position.

3. MEASUREMENT SYSTEM

The measurement system consists of a digital sampling channel probe with a separate transmitter and receiver section. A patent is currently pending on this system. In the measurements presented in this report, the transmitter is placed at fixed locations (cellular base station sites) while the receiver is installed in a measurement van. A well-regulated diesel generator mounted on a trailer is used to power the receiver equipment in the measurement van. Figure 3.1 shows a photograph of the measurement van. In addition to the channel probe, a differential GPS receiver including dead-reckoning sensors was used to record time and vehicle position information of the measurement van.

3.1 Transmitter

Two different PN codes are transmitted at a 10 Mbit/s rate: one at 915 MHz in the 902-928 MHz band and one at 1920 MHz in the 1850-1990 MHz band. This results in a signal bandwidth of 20 MHz and a delay resolution of 100 ns in each band. The maximum measurable delay is 51 μs. Power levels are set to provide 4 W effective isotropically radiated power (EIRP) in the 902-928 MHz band and 50 W EIRP in the 1850-1990 MHz band.

3.2 Receiver

A personal computer is used to control the measurement system receiver. Two vertically polarized monopoles mounted on the roof of the measurement van are used to receive the signals transmitted in the 902-928 and 1850-1990 MHz bands. The system has a processing gain of 27 dB while the noise figures are approximately 11 dB and 8 dB for the 902-928 and 1850-1990 MHz bands, respectively. The channel impulse responses are measured simultaneously in each band and are time-stamped to provide correlation with the measurement van position (stored separately via the GPS and dead-reckoning system).

3.3 Differential GPS System and Dead-Reckoning Sensors

The differential GPS system and dead-reckoning sensors consist of a GPS base station receiver, a GPS mobile receiver, an electronic compass, and a vehicle speed sensor. The GPS base station is installed in a fixed location at the suburban cell site. A mobile GPS receiver is installed along with the dead-reckoning sensors (electronic compass and vehicle speed sensor) in the measurement vehicle. A personal computer located in the measurement van stores data from the GPS receiver and dead-reckoning system. Vehicle position as well as Coordinated Universal Time (UTC) are recorded to the hard disk every second. Under normal operation, time and vehicle position information are obtained from the mobile GPS receiver. If the mobile GPS receiver does not have the required four satellites in view to obtain position information, the dead-reckoning system provides the position information.

Figure 3.1. Photograph of the impulse response measurement van.

4. MEASUREMENT PROCEDURE

The measurement procedure section is divided into subsections on calibration and the measurement system setup, verification, and data collection process followed at each site. Several different types of calibration and system verification were performed, including reference oscillator locking between the transmitter and receiver, amplitude calibration, antenna and feed cable testing, and an over-the-air system check.

4.1 Calibration

The first calibration procedure consisted of tuning the quartz frequency standard located in the transmitter so that its frequency was "exactly" the same as the rubidium frequency standard located in the receiver. This was accomplished by connecting the 10-MHz outputs of each frequency standard to a gain/phase meter and measuring the phase change over a period of 100 s. The amount of phase change over time between the two 10-MHz signals was used to determine the frequency difference between these signals. This method of determining the frequency difference between two continuous wave (CW) signals is much more accurate than using the Lissajous pattern on an oscilloscope. The Lissajous pattern method was initially used to adjust the quartz frequency standard so that its frequency was close to that of the rubidium frequency standard. Although the gain/phase meter does not have good absolute phase accuracy, its phase stability (i.e., ability to measure phase change with time) is excellent and was measured to be less than 0.1 degree in 100 s for 10-MHz inputs. This allows measurement of the frequency difference between two 10-MHz signals to be better than 2.78 parts in 10^{13}. This is better than the short-term stabilities of the reference oscillators, as required for an accurate measurement.

There are three reasons why the oscillator stability and frequency-locking procedures are important. First, it must be assured that the in-phase and quadrature phase components for an individual impulse response do not rotate during data collection. A second reason is that the sampling clock must be accurate enough to ensure that the correct number of samples are taken within the 511-bit PN code word. If this condition is not met, the correlation noise floor increases thereby decreasing the interval of discrimination (amplitude difference between the correlation peak and the peak of the noise) in the impulse response. Finally, it must be ensured that the phase between each sequentially taken impulse response does not change appreciably due to oscillator drift (to ensure accuracy of Doppler shift information). The most stringent requirement out of all three cases is in ensuring the accuracy of Doppler shift information. The data taken with 1.5 ms between successive impulse responses was used to preserve Doppler shift information. To obtain a Doppler shift accuracy of 1 Hz, oscillator stabilities of 5.21 parts in 10^{10} are required. Both of the frequency standards used in these measurements easily met this requirement and the accuracy of setting the frequency difference between the two oscillators also met this requirement.

The second type of system calibration that was performed was a receiver amplitude calibration. This entailed connecting the transmitter directly to the receiver via a coaxial cable, with a variable attenuator inserted between the transmitter and receiver to control the amplitude of the signal input into the receiver. For each RF input power level into the receiver (in 10-dB steps), from the receiver's 0.5-dB compression point until the receiver could only detect noise, a power delay profile (PDP) was obtained. The PDP is the magnitude squared of the measured complex impulse response. The results of this calibration provided a series of PDPs at varying RF input power levels to the receiver for both the 902-928 and 1850-1990 MHz channels. An example of these calibration PDPs for high-level input signals into the receiver for the 18501990 MHz band is shown in Figure 4.1. From this PDP, the interval of discrimination (ID) is seen to be approximately 47 dB. The ID is the difference in power between the correlation peak

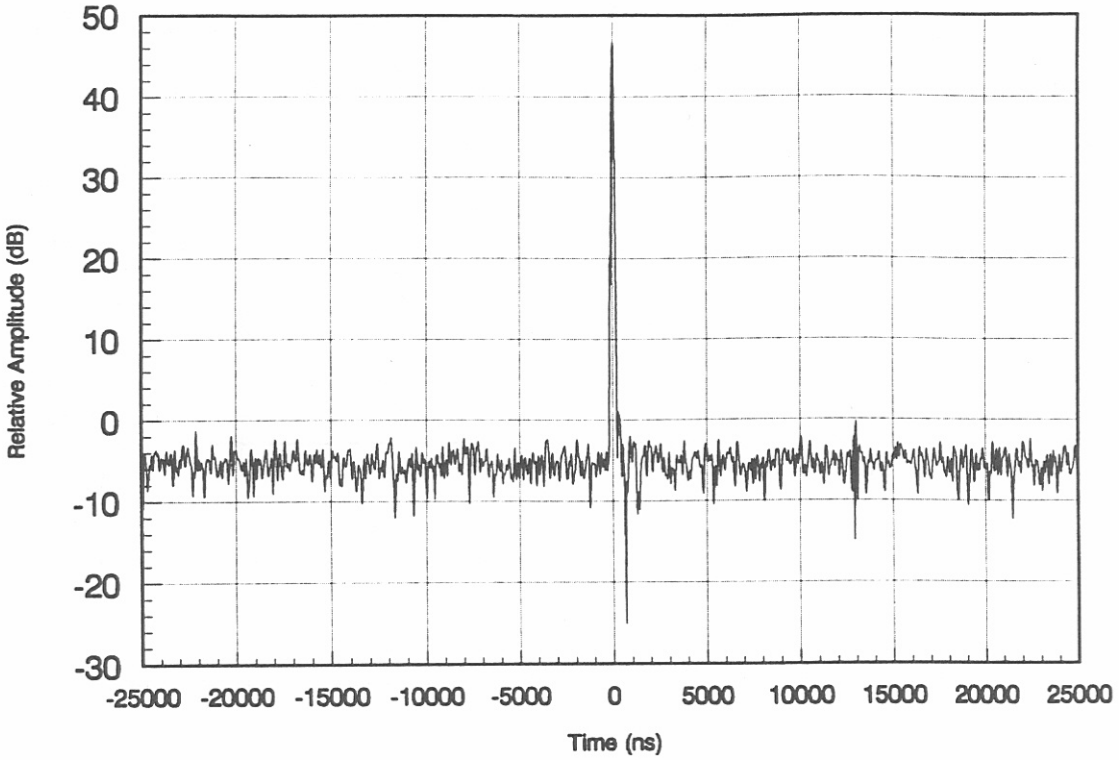

Figure 4.1 Example calibration power delay profile for the 1850-1990 MHz band.

and the peak noise level in the PDP. This approaches the theoretical limit of a 9-bit PN code generator given by $20*\log_{10}(2^n-1) \approx 54$ dB where n = 9. By averaging the noise, the ID of the calibration PDP shown in Figure 4.1 would even more closely approach the theoretical limit. From the calibration PDPs it is noted that as the RF input power into the receiver decreases to roughly -60 dBm, the ID does not decrease. As the RF input power into the receiver decreases below -60 dBm, the ID decreases due to system noise. The processing gain from a 9-bit PN code generator is given as $10*\log_{10}(2^n-1) \approx 27$ dB. This means that when the RF input power

into the receiver is equal to the system noise of the receiver, the correlation peak will be 30 dB above the average noise level. This occurs when the RF input power is in the -90 to -95 dBm range. The presence of multipath even further reduces the ID.

The total power in each calibration PDP was computed providing a correlation between input RF power into the receiver and the total power in the PDP. Table 4.1 shows this correlation.

Table 4.1 Correlation Between Receiver RF Input Power and Total Power in the PDP

902-928 MHz Band		1850-1990 MHz Band	
Receiver RF Input Power (dB)	Total Power in PDP (dB)	Receiver RF Input Power (dB)	Total Power in PDP (dB)
-31	72.27	-35	71.49
-41	63.72	-45	62.83
-51	53.83	-55	52.38
-61	43.66	-65	42.67
-71	33.82	-75	32.64
-81	23.94	-85	22.94
-91	17.56	-95	16.52
-101	14.94	-105	14.20
-111	15.49	-115	14.22
-121	14.94		

Note that the total power in the PDP decreases approximately by the same amount as the RF input power into the receiver until the RF input power reaches -81 dBm and -85 dBm for the 902-928 and 1850-1990 MHz bands, respectively. As the RF input power decreases beyond these points, the total system noise power becomes an appreciable part of the total power in the PDP. The benefits of this type of calibration are the ability to verify proper operation of the measurement system; provide a relationship between received signal power, the PDP, and the total power in the PDP; and allow approximate determination of the input compression point and noise figure of the receiver from the PDP.

In order to complete the calibration of the entire system, the antenna gains and the attenuation of the antenna feed cables for both the transmitter and receiver had to be determined. In addition, the correct operation of both the antennas and feed cables had to be ensured.

Antenna gain was provided for all of the transmitter and receiver antennas by the antenna manufacturers. The insertion loss of the antenna feed cables was measured as well as the return loss of the antennas. These were checked to be sure that they met specifications. The antennas were then connected to the corresponding antenna feed cables and the return loss at the end of the feed cables was determined. The return loss measured here was compared to the return loss of the antennas plus two times the insertion loss of the corresponding feed cables. If these two values agreed, the antenna and feed cable performance was verified.

4.2 Measurement System Setup, Verification, and Data Collection Process

The calibration, system verification, and setup procedures described here were performed in the morning each day before measurements began. Measurements were made at four different cell sites. At two of the sites, two different transmit antenna types were used. Measurements took approximately one day to complete for each cell site/antenna combination.

The initial procedures about to be described were performed upon arrival at the first cell to be tested in Philadelphia (suburban cell). Before calibration began, the transmitter and receiver equipment were warmed up for one-half hour. The quartz frequency standard in the transmitter was adjusted so that its frequency matched that of the rubidium frequency standard in the receiver, according to the procedure described in Section 4.1. The next test performed was to determine the potential interfering signals in or near both measurement frequency bands. The transmitter was disconnected and turned off while the receiver inputs were connected to the vertically polarized monopoles mounted on the measurement van. The receiver spectrum analyzers were set up in sweep mode to observe and display frequencies from 865 to 965 MHz and from 1870 to 1970 MHz. No significant signals were seen in the 1870 to 1970 MHz range but some strong interferers were observed at 928 and 931 MHz. A tunable notch filter was adjusted until maximum attenuation of these signals was obtained. This filter was then set to hold this particular frequency response. The transmitter and receiver were then connected directly via a coaxial cable and a variable attenuator. The receiver amplitude calibration (as described earlier) was performed with the results compared to the initial calibration completed after system development. These results showed that the measurement system was operating properly in that the PDPs at each RF input power level into the receiver and the system noise level were as expected.

Similar procedures were used at all sites with a couple of exceptions. The frequency ranges 865-965 and 1870-1990 MHz were observed to ensure that no strong interferers were present. The notch filter did not need to be readjusted since any interfering signals seen were greatly attenuated. The full receiver amplitude calibration was not performed for sites other than the initial (suburban) site. Instead, the receiver amplitude calibration was checked at a couple RF input amplitudes into the receiver to ensure proper system operation.

The following procedures were then performed at each site. First, the transmitter and receiver antennas and antenna feed cables were tested according to the procedure discussed in Section 4.1. The power output of the transmitter was adjusted based on the known cable losses

and antenna gains to provide the power levels specified in Section 3.1 for each frequency band. A power meter was used to provide a precise measurement of the output power of the wideband transmitter signals. The antennas were connected to both the transmitter and receiver and the measurement van was positioned on the ground within approximately 15 m of the base of the transmitter. The transmit antennas at each site were at least 30 m above the ground, so that the separation between the transmit and receive antennas was substantial. An over-the-air test, which was primarily qualitative in nature, was then performed to test the proper functioning of the entire transmitter/receiver measurement system including the antennas and antenna feed cables. For this test, the transmitter was turned on and the received signals were checked for proper frequency and amplitude. Data were captured for both frequency bands and the corresponding PDPs were compared to expected results to determine if the entire system was operating properly. The transmitter was kept operating while the rest of the setup procedures were performed and was not turned off until the measurements in that cell were completed.

The mobile GPS receiver and dead-reckoning system located in the measurement van were set up for automatic time and vehicle position data acquisition. The measurement van was moved to the beginning of the first route selected for measurement within the cell. Three versions of the data acquisition and control software were used to run the impulse response measurement system. The three versions corresponded to the three different data acquisition schemes available as discussed in Section 2 of this report. The type of data acquisition was chosen by the system operator and the appropriate program was invoked to prepare the measurement system for data collection. First, under computer control, the receiver hardware was initialized. Based upon the received signal levels, the amplitude sensitivity of both channels of the receiver was automatically set by an autoscaling procedure. The sensitivity of each channel was set independently. The system operator had the option of overriding the automatic amplitude sensitivity settings and entering those desired. The system operator was then prompted for information to be stored in the data file header. This information included the cell number and description; the route number within the cell; and the transmit antenna type, polarization, and height. The computer's clock was then automatically set to Coordinated Universal Time (UTC) using information from the GPS receiver.

After these setup procedures, the data acquisition was initiated and the measurement van began travelling along the selected route. Each succession of impulses (three or ten depending on the acquisition type) was time-stamped using the computer clock to allow correlation between the data and the vehicle position. Time and vehicle position from the GPS receiver and dead-reckoning system were stored every second in a separate file. The control software monitored signal levels on both frequency channels and if either signal level was too low or too high for adequate digitization an alarm would sound and the corresponding data on both channels would not be recorded. If the signal levels were persistently too low or too high, the measurement van was stopped and the autoscale procedure was executed again before restarting data acquisition. Data of appropriate signal level were stored on the computer hard disk. The measurement environment as seen from the front windshield of the van was recorded on video tape as the van moved along the selected measurement routes in each cell. Comments and observations made verbally by the measurement personnel were also recorded on the videotape. The video tapes were time-stamped allowing correlation between the data and the measurement environment at any time. After all of the data had been acquired for the day, the data were checked by looking at selected impulse responses taken that day. Assured that the data were sound, the data were backed up onto optical disk.

5. MEASUREMENT LOCATIONS

Before the data analysis is discussed and the results are presented, a description of the cell environments is given. Directionality of the transmit antennas in each cell is given. Directionality as used in this paper refers to that in the azimuthal plane only.

Figure 5.1 shows a map of the urban high-rise cell with the routes marked where the measurements were taken. The transmitter was located at 1500 Locust St. in central Philadelphia, PA. This area consists of closely spaced buildings with heights typically exceeding 40 stories. In this cell, measurements were taken using vertically polarized transmit and receive antennas. Additional measurements, taken along the same routes, were made using circularly polarized transmit antennas (the receive antennas were still vertically polarized). Both types of transmit antennas were directional with a 3-dB beamwidth of approximately 90 degrees. The antenna beamwidth is shown on the map as heavy lines emanating from the transmitter. The transmit antennas were mounted on the 48th floor of an office building (approximately 167 m aboveground).

The transmitter for the urban cell was located at 4022 Chestnut St., also in Philadelphia. This cell is characterized by three- to four-story buildings throughout most of the area. The transmit antennas were mounted on a tower 30 m aboveground. In this cell, measurements were only taken using the vertically polarized transmit and receive antennas. As in the urban high-rise cell, the transmit antennas were directional with a 3-dB beamwidth of 90 degrees. This beamwidth is also shown on the map as heavy lines emanating from the transmitter. This cell site, along with the measurement routes travelled, are shown in Figure 5.2.

The suburban cell consisted of both residential and small business areas with typical building heights of no more than two stories. The transmitter for this cell was located at 508 S. Lenola Rd. in Mapleshade, NJ. Its transmit antennas were mounted on a tower approximately 60 m aboveground. As in the urban high-rise cell, measurements were taken using both vertically and circularly polarized transmit antennas. Here the vertically polarized transmit antennas were omnidirectional while the circularly polarized transmit antennas were directional with a beamwidth of 90 degrees. This difference in antenna directionality should be kept in mind when comparing the data taken with both transmit antenna polarizations in this cell. A map of this cell depicting the measurement routes followed is given in Figure 5.3. The map also shows the 3-dB beamwidth of the circularly polarized transmit antennas as heavy lines emanating from the transmitter.

The transmitter for the semi-rural cell was located at the corner of Route 213 and Flowers Mill Road in Langhorne, PA. The environment in this cell consisted primarily of open spaces and farmland, although there were some small business and residential properties. Transmitter antenna heights for this cell were approximately 36 m. Measurements were made in this cell using only the vertically polarized transmit and receive antennas. The transmit antennas were omnidirectional. Figure 5.4 shows a map of this cell and the measurement routes.

Terrain in all cells was relatively flat but included some rolling hills and valleys. Most areas, except for those within the urban high-rise cell, included dense groves of deciduous trees in full leaf (Tanis, 1993).

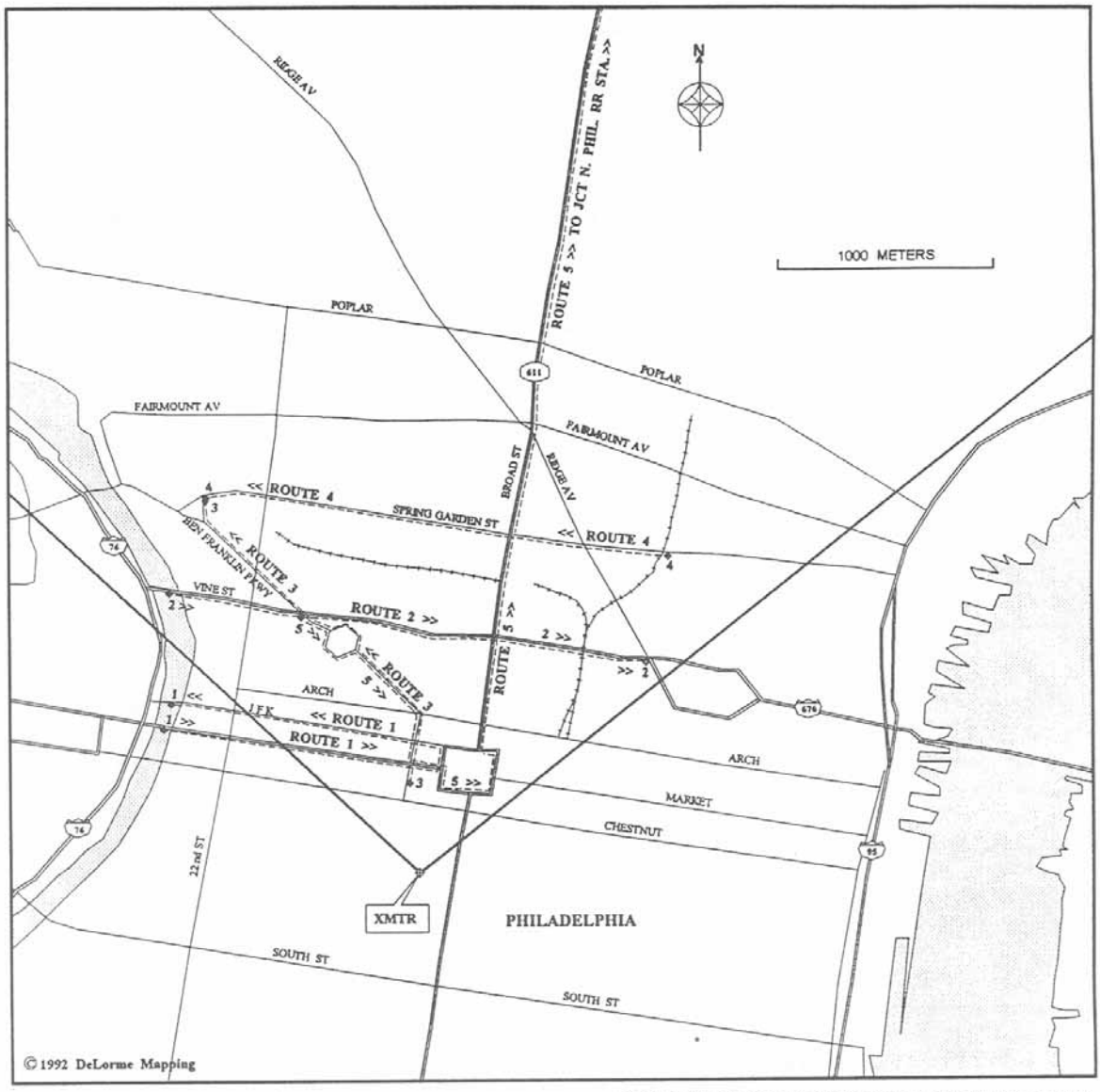

MAP FROM DELORME'S MAPEXPERT, FREEPORT, MAINE.

Figure 5.1. Measurement routes in the urban high-rise cell.

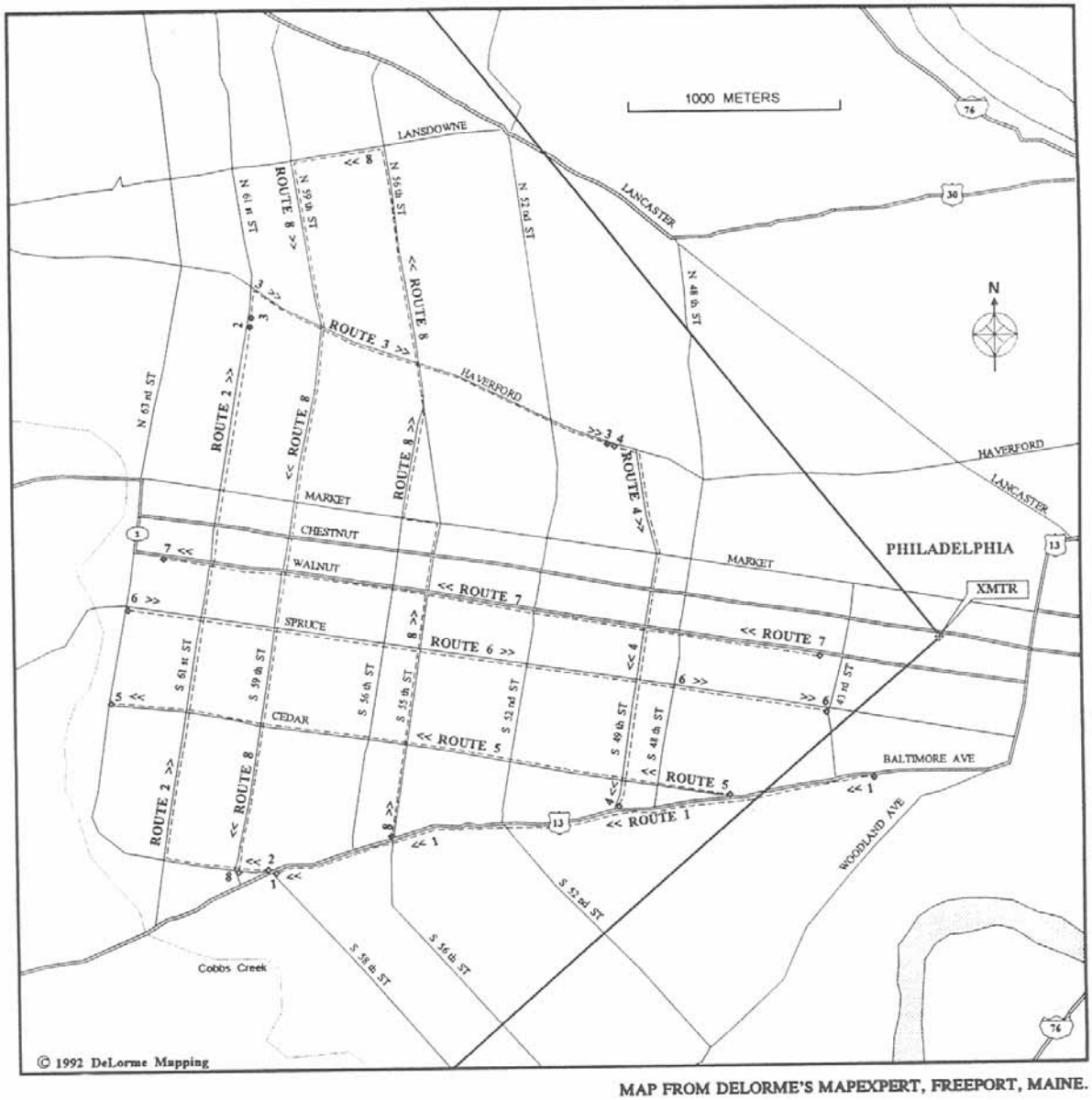

MAP FROM DELORME'S MAPEXPERT, FREEPORT, MAINE.

Figure 5.2. Measurement routes in the urban cell.

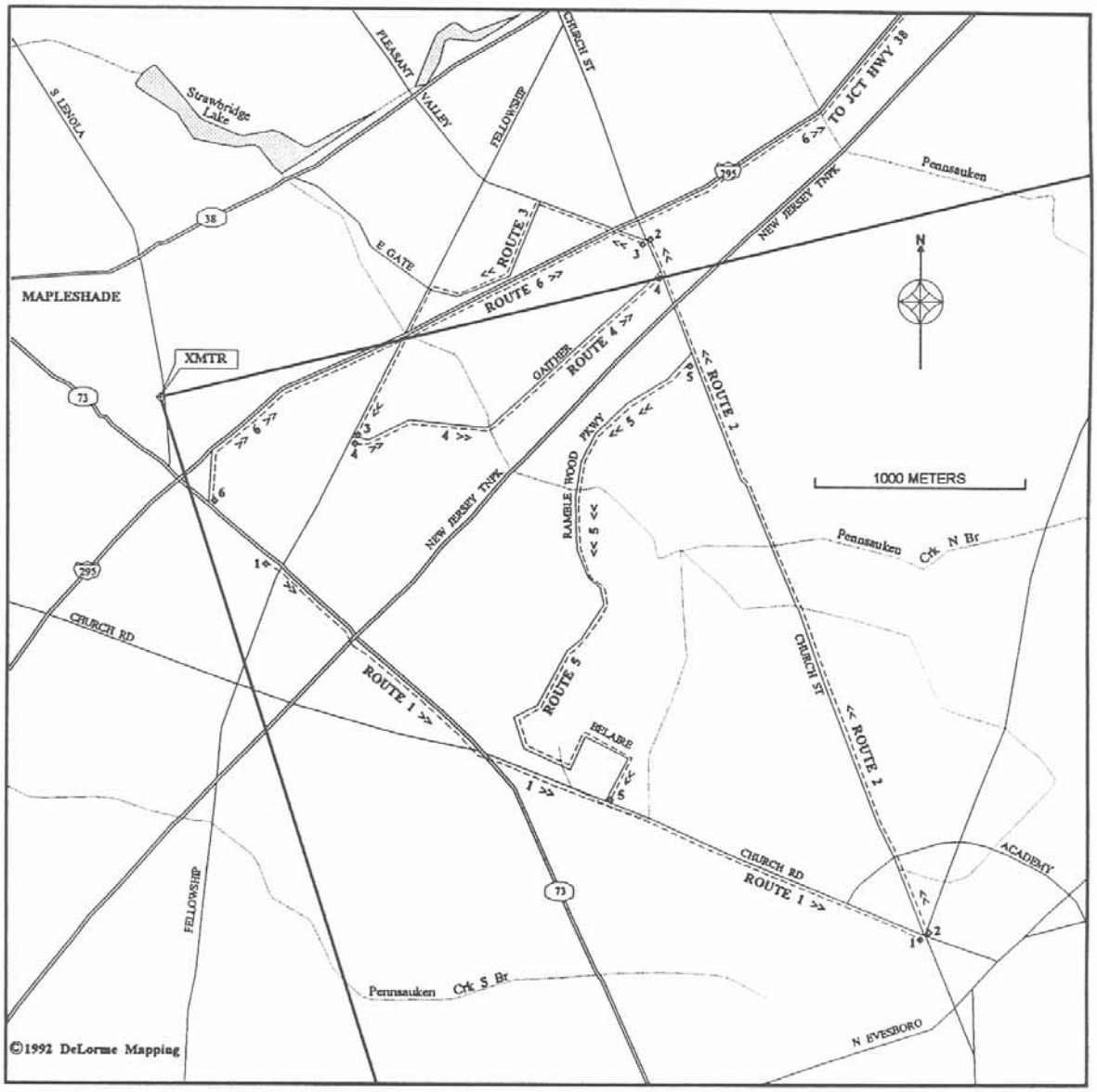

Figure 5.3. Measurement routes in the suburban cell.

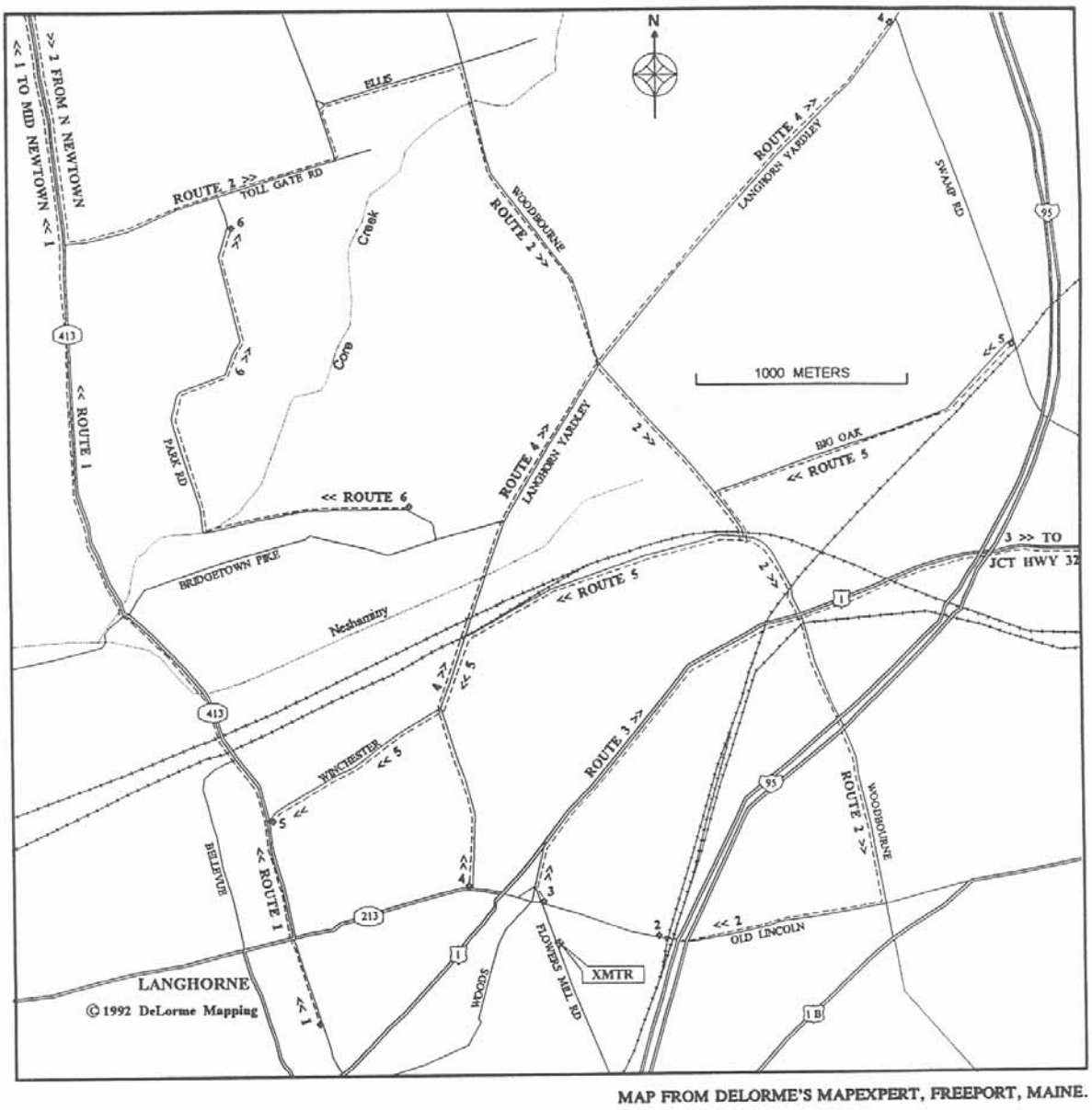

Figure 5.4. Measurement routes in the semi-rural cell.

6. DATA ANALYSIS METHODS AND RESULTS

The impulse response data are analyzed by generating several types of statistics. These statistics include probability density and cumulative distribution of RMS delay spread and correlation bandwidth as well as various other multipath power statistics. In this section, a detailed explanation of how these statistics were generated is given along with a presentation of the results. All of these statistics are computed for each of 12 different data sets. The 12 data sets are listed in Table 6.1 and are comprised of data taken using different combinations of cell type, antenna polarization, and frequency. All of the statistics are computed from averaged PDPs (APDPs). Therefore, the first step in the data analysis process, common to all of the statistics, was to develop the APDPs.

Table 6.1. Data Sets for Computation of Statistics

Data Set #	Cell Type	Transmit Antenna Polarization	Frequency (MHz)
1	Semi-Rural	Vertical	915
2	Semi-Rural	Vertical	1920
3	Suburban	Vertical	915
4	Suburban	Vertical	1920
5	Suburban	Circular	915
6	Suburban	Circular	1920
7	Urban	Vertical	915
8	Urban	Vertical	1920
9	Urban High-Rise	Vertical	915
10	Urban High-Rise	Vertical	1920
11	Urban High-Rise	Circular	915
12	Urban High-Rise	Circular	1920

As mentioned in Section 2 of this report, the only data used for analysis were those taken using the fast data acquisition scheme. In this scheme, every 0.5 s, a rapid succession of three PDPs was taken. Spatial distance between each PDP within the succession of three ranged from approximately 1 to 3 cm. An APDP is determined from these three PDPs according to the following procedure. Initially, the total signal power is determined for each of the three PDPs

and the PDP with the greatest total power is identified. Any of the three PDPs with a total power 10 dB or more below the PDP with the greatest total power is tagged as invalid and excluded from processing. Therefore, a set of valid PDPs within the succession of three PDPs could consist of one, two, or three PDPs.

In order to compute an APDP, alignment in time between all valid PDPs (within a succession of three PDPs) is required. Obviously, if only one valid PDP exists, alignment and averaging are not necessary. Alignment is accomplished by performing cross correlations between consecutive valid PDPs. The second valid PDP is aligned with the first valid PDP by shifting the second one in time according to the results of the correlation. If a third valid PDP exists, it is then aligned with the second valid (previously aligned) PDP. Once aligned, all of the valid PDPs (within the succession of three PDPs) are averaged together to give an APDP. This type of alignment was utilized to obtain average values of power for the same delayed signals. Since taking measurements over such a large area required a sizable amount of data storage, only a succession of three PDPs could be taken (and thus averaged) in order to keep the data processing effort manageable.

The received signal levels obtained in the measurements tended to be relatively low (approximately -90 dBm) in many locations due to the large distances between the transmitter and receiver, limited transmitter power as required by the experimental license, and shadow fading. Due to these relatively low signal levels and the presence of multipath, an ID of only 20 dB could be guaranteed from APDPs taken in many locations. Because of this and also to treat APDPs of varying IDs on an equivalent basis, only delayed signals within 20 dB of the peak value in the APDP were counted as significant for the computations. The APDPs are used as the basis for computing the RMS delay spread, multipath, and correlation bandwidth statistics. To ensure that noise was not included in the statistical computations, an APDP was only considered valid (for inclusion in the statistics) if its ID was 23 dB or greater. This assured that samples of the APDP up to 20 dB below the peak received signal would be actual delayed signals and not noise (by providing a 3 dB buffer between the peak of the noise and the region where the amplitude of delayed signals was considered significant). If the APDP had an ID less than 23 dB, this APDP, as well as the APDP that was computed from PDPs taken simultaneously in the other frequency band, were not counted in the statistics. This guaranteed that the number of APDPs for each frequency band was the same.

Alignment in time between each APDP was then addressed. All of the valid APDPs (i.e., those APDPs having at least one sample 23 dB or more above the peak noise value and having the corresponding APDP on the other frequency band also meet this criterion) are then shifted in time such that the first perceptible received copy of the transmitted signal is set to zero time. This is accomplished by finding the first sample in the APDP, within the region 25 μs before the peak signal, whose power is within 20 dB of the peak signal level. After this alignment procedure, the APDPs were ready to be utilized in the computation of RMS delay spread, multipath, and correlation bandwidth statistics. Note that when the term APDP is used in the rest of this report, that it implies a valid and aligned APDP.

For each data set, the number of APDPs available for use in the computation of the statistics is called the sample size. The sample size is a selected number of individual values (in this case APDPs) within an entire population (total possible number of individual values [APDPs]). Statistics computed from a sample size represent an approximation to those that would be obtained (if possible) from the entire population. The larger the sample size, the better the computed statistics represent the behavior of the entire population. Therefore, the statistics generated in this paper, as any statistics computed from measurements, are representative of the entire population within some error bounds. These error bounds are a function of the sample size.

Many conclusions in this paper are made from sample cumulative distributions of RMS delay spread and correlation bandwidth. The error bounds about the sample cumulative distribution in which the cumulative distribution of the population will lie for a given confidence level can be easily computed (Dixon and Massey, 1969). These bounds are given in Table 6.2 for each combination of cell type and transmit antenna polarization for both an 80% and 99% confidence level. The corresponding sample size is also given in this table.

Table 6.2 Error Bounds on the Sample Cumulative Distributions

Cell Type/ Antenna Polarization	Sample Size	Error Bounds (in probability units)	
		80% Confidence	99% Confidence
Semi-Rural/ Vertical	1118	±0.032	±0.049
Suburban/ Vertical	1537	±0.027	±0.042
Suburban/ Circular	1023	±0.034	±0.051
Urban/ Vertical	539	±0.046	±0.070
Urban High-Rise/ Vertical	901	±0.036	±0.054
Urban High-Rise/ Circular	798	±0.038	±0.058

For an example of the use of Table 6.2, consider the semi-rural cell using vertical polarization. One can be 80% confident that the population cumulative distribution falls within a band of ±0.032 about the sample cumulative distribution.

6.1 RMS Delay Spread

RMS delay spread is a parameter used to characterize the impulse response of a radio channel. This parameter is convenient since it describes an entire impulse response with a single number [Devasirvatham, 1987]. Therefore, it is useful in statistically describing a set of many impulse responses. It takes into account the number of delayed signals, the amplitude of each delayed signal, and the time of arrival of each delayed signal relative to the first received signal.

Since delayed signals within 20 dB of the peak value in the APDP are the only ones counted as significant, samples within each APDP that are more than 20 dB below the maximum signal level are set to zero for the RMS delay spread computation. RMS delay spread (in s) is computed for each of the APDPs using (Cox and Leek, 1975; Cox, 1972a and b)

$$S = \left[\sum_{k=1}^{N} (\tau_k - d_m)^2 \; P(\tau_k) \Big/ \sum_{k=1}^{N} P(\tau_k) \right]^{\frac{1}{2}}$$

where N is the number of sample data points in the APDP, τ_k is the time delay (in s) of the k^{th} sample in the APDP relative to the time of occurrence of the first perceptible reception of the transmitted signal, and $P(\tau_k)$ is the value of the APDP at a time delay of τ_k. The average excess delay d_m (in s) is given as

$$d_m = \sum_{k=1}^{N} \tau_k \; P(\tau_k) \Big/ \sum_{k=1}^{N} P(\tau_k).$$

For each of the 12 data sets listed in Table 6.1, the probability density and cumulative distribution of RMS delay spread are computed.

Figures 6.1a-6.4a show the probability densities of RMS delay spread for 915 MHz using vertically polarized transmit antennas for the semi-rural, suburban, urban, and urban high-rise cells, respectively. Figures 6.1b-6.4b show the corresponding statistics for 1920 MHz. The probability density functions shown here are approximate and are determined from histograms with 25-ns bins. Values on each of these plots represent the percentage of APDPs for a given data set having an RMS delay spread that falls within a particular 25-ns bin. In the semi-rural, suburban, and urban cells, the probability densities of RMS delay spread are similar and show a somewhat exponential decrease in the percentage of APDPs as the RMS delay spreads vary from 0 to 0.5 μs. For the urban high-rise cell, the probability density functions (Figures 6.4a-b) show a more uniform distribution along with larger values of RMS delay spread.

Figures 6.lc-6.4c show the cumulative distributions of RMS delay spread for each of the cells using the vertically polarized transmit antennas. Both frequency bands are shown on each plot to facilitate the comparison of propagation behavior between the two bands. The

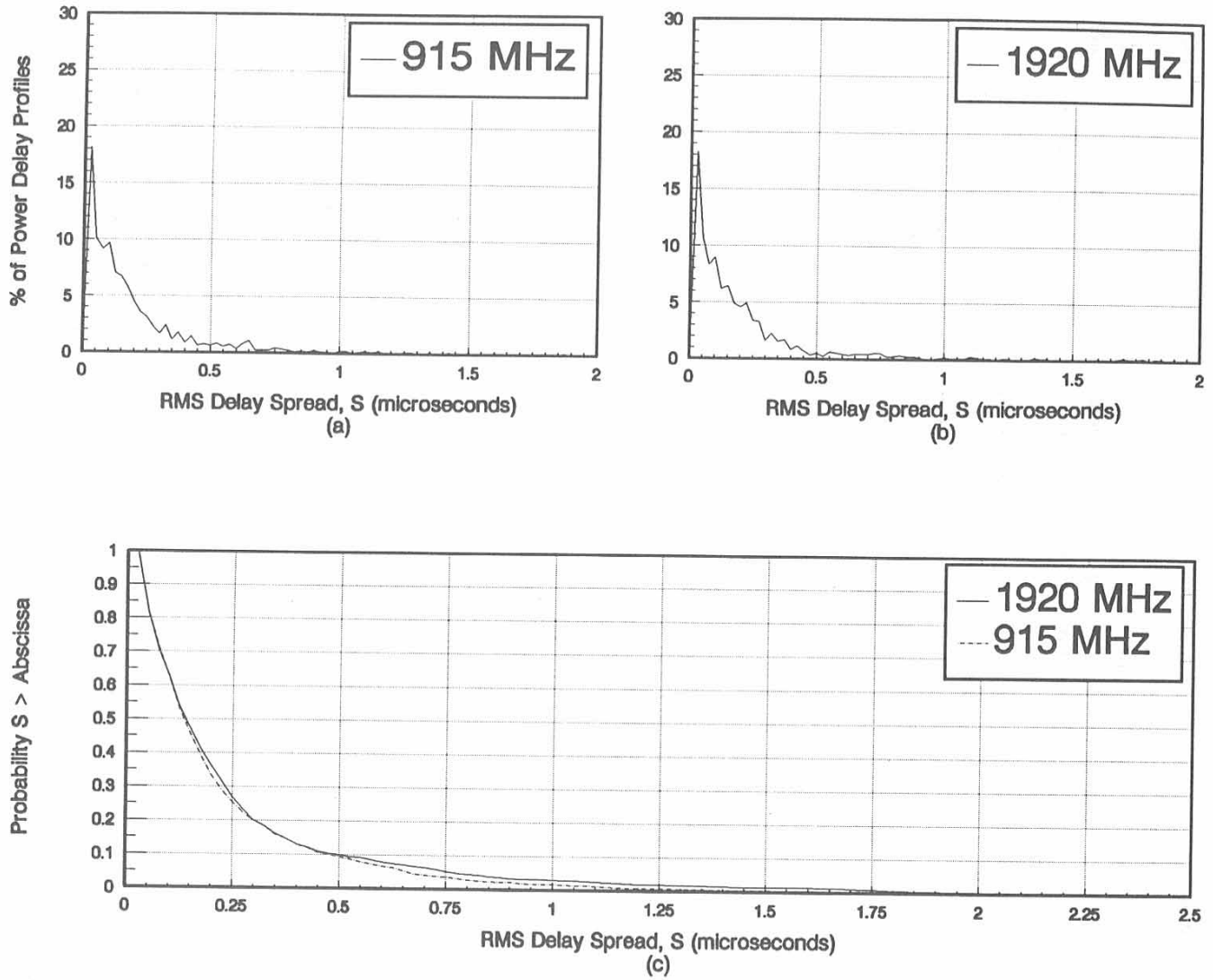

Figure 6.1. **Probability density (a-b) and cumulative distribution (c) of RMS delay spread for the semi-rural cell using vertically polarized transmit antennas.**

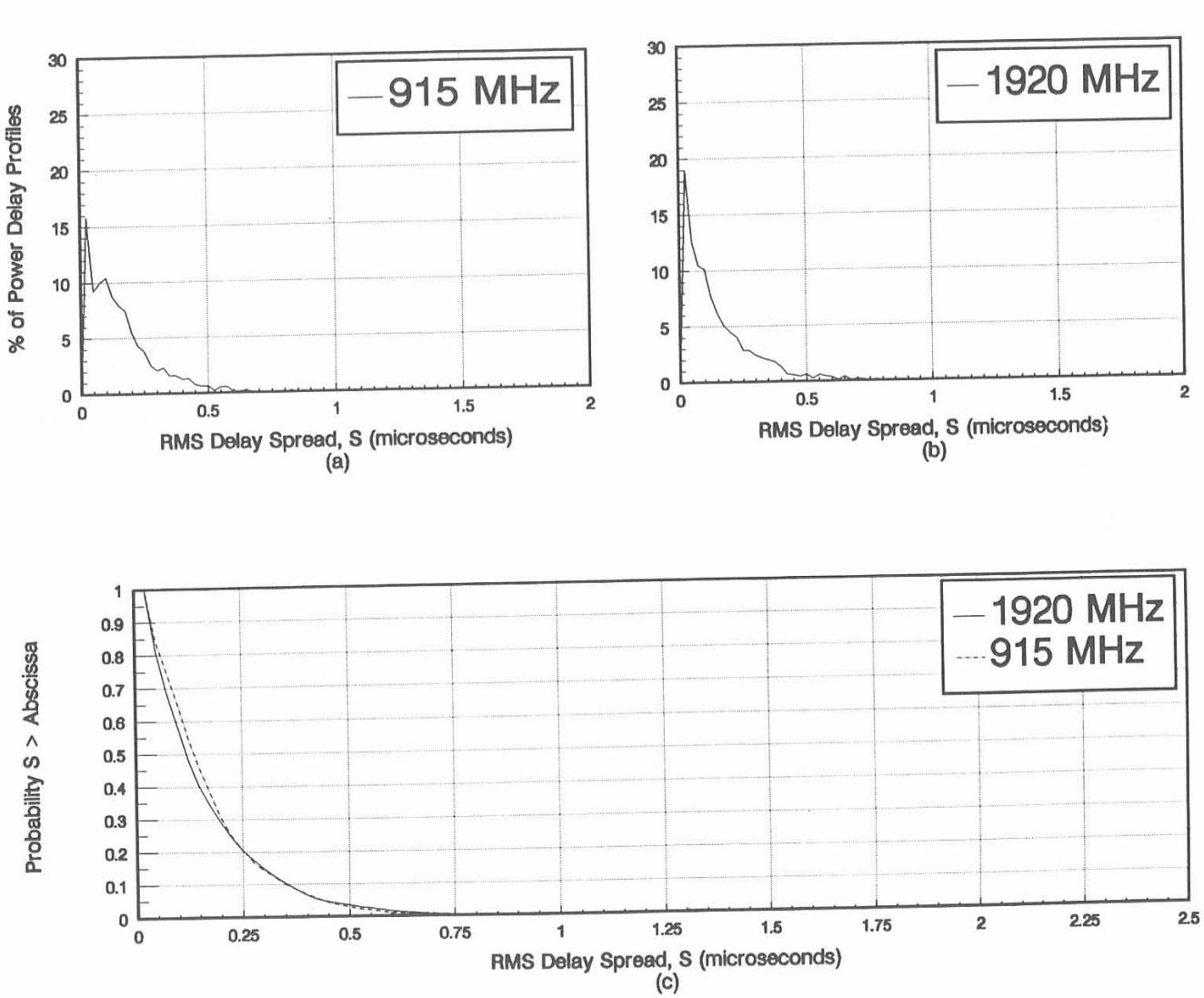

Figure 6.2. **Probability density (a-b) and cumulative distribution (c) of RMS delay spread for the suburban cell using vertically polarized transmit antennas.**

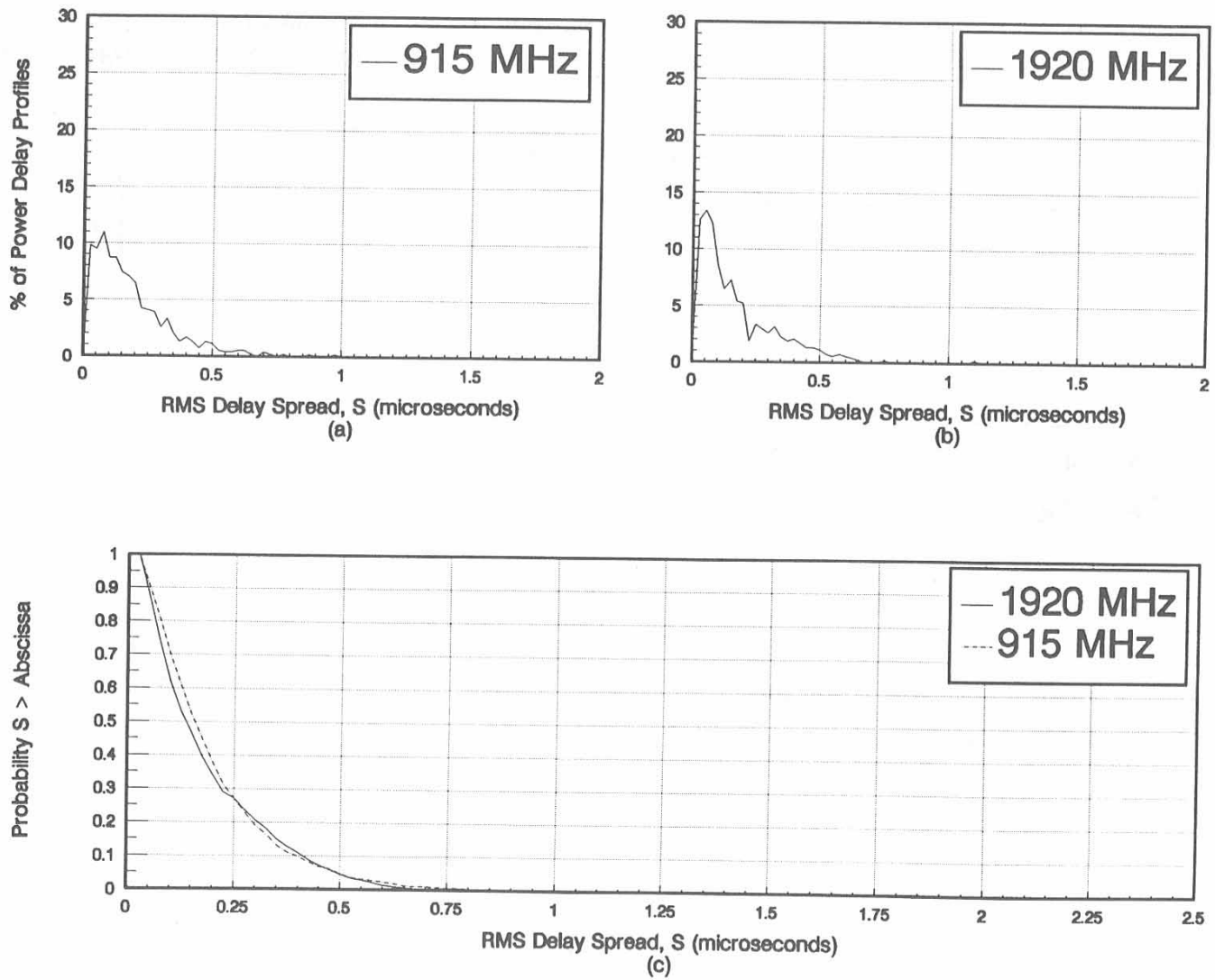

Figure 6.3. **Probability density (a-b) and cumulative distribution (c) of RMS delay spread for the urban cell using vertically polarized transmit antennas.**

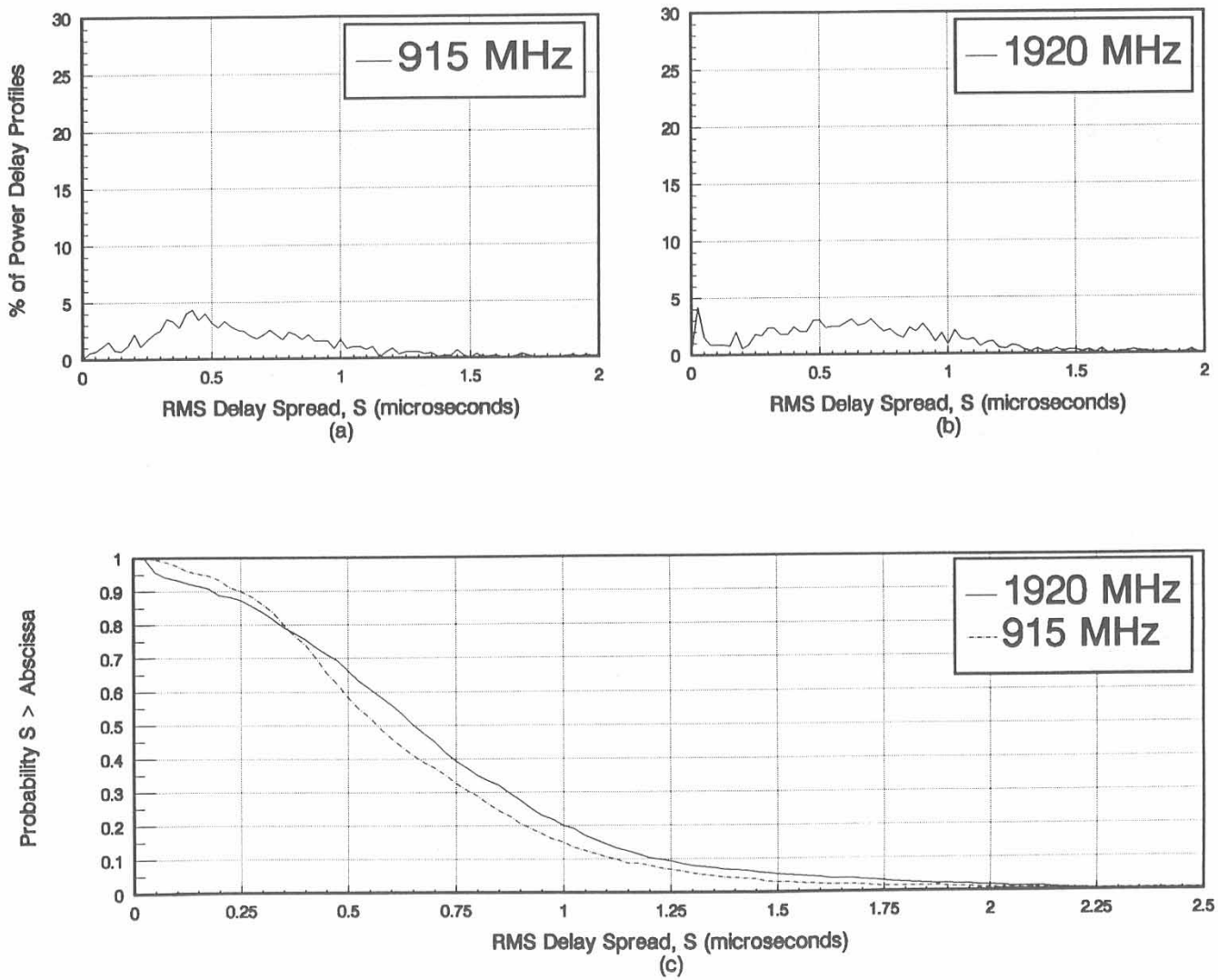

Figure 6.4. **Probability density (a-b) and cumulative distribution (c) of RMS delay spread for the urban high-rise cell using vertically polarized transmit antennas.**

propagation behavior between the two frequencies appears to be quite similar in the semi-rural, suburban, and urban cells. Additionally, the cumulative distributions of RMS delay spread between all three of these cells are very similar. The semi-rural cell does show a very low probability of exceeding RMS delay spread values between 0.75 μs and 1.75 μs. This does not show up in the cumulative distributions for the suburban and urban cells. This phenomenon may be due to hilly terrain in the semi-rural environment. Considering the error bounds on the cumulative distributions, a much larger sample size would be required to verify this phenomenon for the entire population.

There is marked difference in the cumulative distribution between the urban high-rise cell and the other cells. The RMS delay spreads for the urban high-rise cell are substantially larger. This occurs because the tall buildings and high transmit antennas tend to provide more and longer propagation paths with less path loss than in the other cells. There is a small difference between the cumulative distributions for the two frequencies in the urban high-rise cell. Considering error bounds, however, there may be no real difference between the population cumulative distributions of these two frequency bands.

Separate measurements using circularly polarized transmit antennas (the receive antennas were still vertically polarized) were taken along the same routes as the measurements using the vertically polarized transmit antennas. Figures 6.5 and 6.6 show the probability densities and cumulative distributions of RMS delay spread for the suburban and urban high-rise cells respectively, using the circularly polarized transmit antennas. In comparing the cumulative distribution plots (Figures 6.5c and 6.6c) with the corresponding plots using vertically polarized transmit antennas (Figures 6.2c and 6.4c), some interesting trends are observed. Compare the urban high-rise cell plots (Figures 6.4c and 6.6c). It is seen that the probability of the RMS delay spread being greater than the abscissa is somewhat lower with the circularly polarized transmit antennas than with the vertically polarized transmit antennas for 1920 MHz. For the most part, this phenomenon is also evident when comparing the suburban cell plots (Figures 6.2c and 6.5c). In the urban high-rise and suburban cells, the cumulative distribution curves do not change much due to transmit antenna polarization for 915 MHz. These results suggest that the detrimental effects of multipath propagation may be reduced by using circular polarization in the transmit antennas of a PCS system operating in various macrocellular environments. Additionally, the results suggest that these benefits obtained may be more significant for 1920 MHz than for 915 MHz. Further polarization studies are recommended to investigate these possible benefits.

A possible reason why transmitting with circular polarization and receiving with vertical polarization may reduce multipath is now discussed. When a circularly polarized wave reflects off of an object, the vertically polarized component of the resultant wave may be smaller than the same component created when a vertically polarized wave reflects off of the same object. If this does occur, circularly polarized waves travelling over reflected paths would then be received with lower amplitude by a vertically polarized antenna than vertically polarized waves travelling over the same paths. Less multipath would then be seen for transmitting with circular polarization.

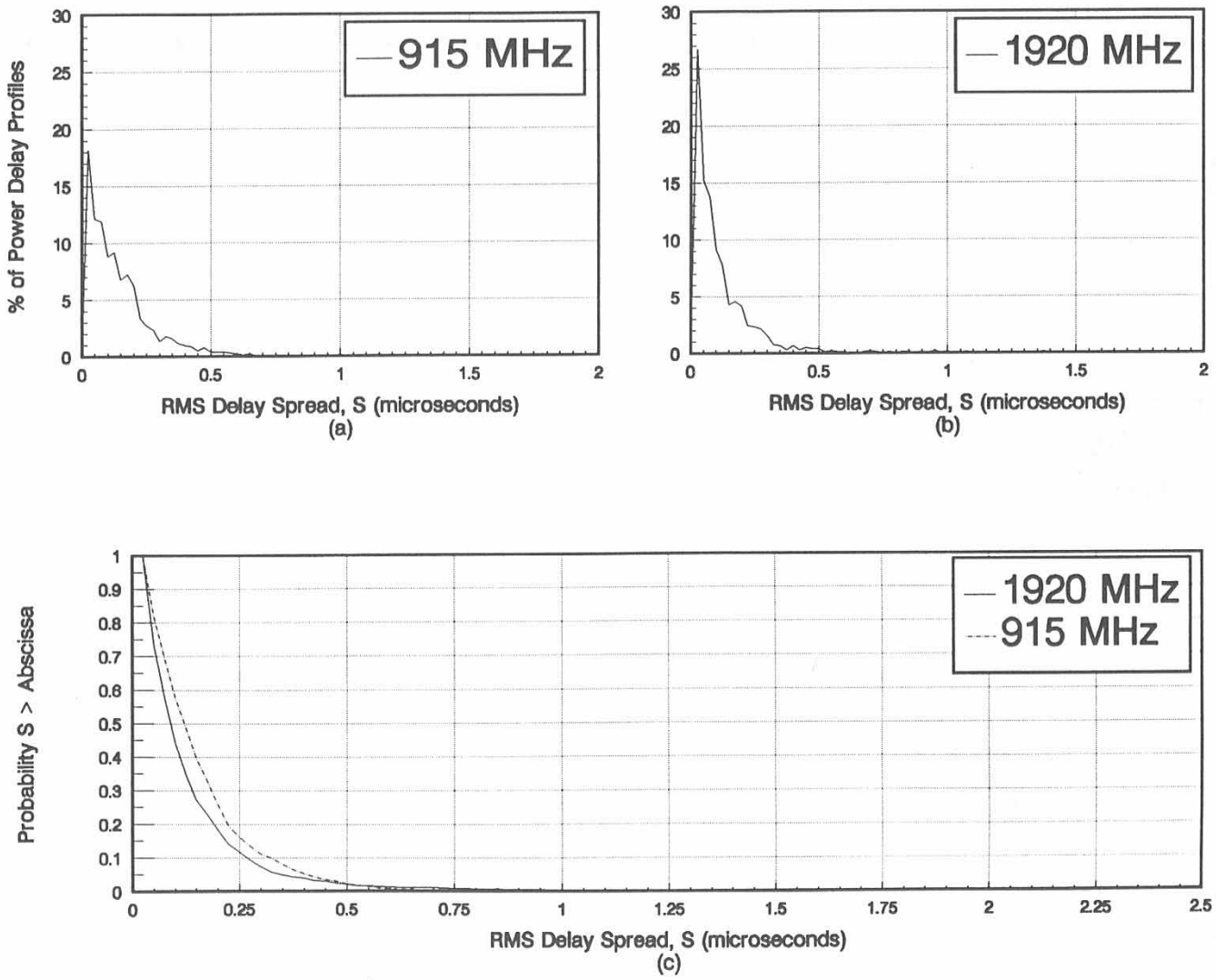

Figure 6.5. **Probability density (a-b) and cumulative distribution (c) of RMS delay spread for the suburban cell using circularly polarized transmit antennas.**

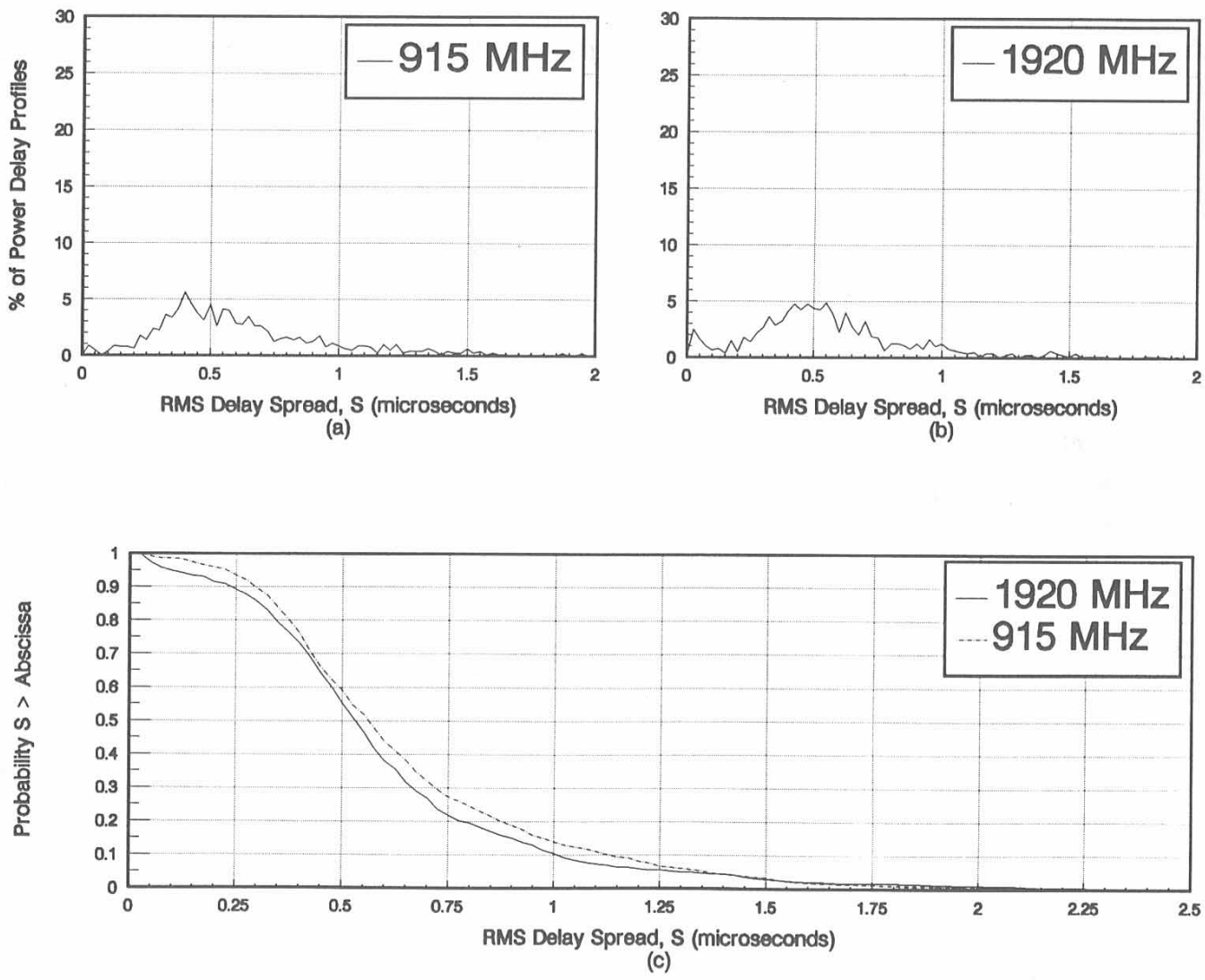

Figure 6.6. **Probability density (a-b) and cumulative distribution (c) of RMS delay spread for the urban high-rise cell using circularly polarized transmit antennas.**

Tables 6.3 and 6.4 provide for a quantitative comparison of the cumulative distributions of RMS delay spread between the various cells and between both antenna polarizations for 1920 MHz and 915 MHz respectively. These tables show RMS delay spread values (in μs) for which there is a fixed probability of exceeding. For example, there is a probability of 0.1 that the RMS delay spread of the 1920 MHz signal will exceed 1.21 μs in the urban high-rise cell using vertical polarization. On the other hand, there is a probability of 0.1 that the RMS delay spread of the 1920 MHz signal will exceed 0.41 μs in the urban cell using vertical polarization.

Table 6.3. Comparison of RMS Delay Spread Values Exceeded (in μs) for 1920 MHz

Cell Type/Antenna Polarization	Probability of Exceeding RMS Delay Spread		
	0.5	0.2	0.1
Semi-Rural/ Vertical	0.14	0.30	0.50
Suburban/ Vertical	0.12	0.25	0.35
Suburban/ Circular	0.09	0.19	0.27
Urban/ Vertical	0.14	0.31	0.41
Urban High-Rise/ Vertical	0.65	1.00	1.21
Urban High-Rise/ Circular	0.53	0.78	1.01

Table 6.4. Comparison of RMS Delay Spread Values Exceeded (in μs) for 915 MHz

Cell Type/Antenna Polarization	Probability of Exceeding RMS Delay Spread		
	0.5	0.2	0.1
Semi-Rural/ Vertical	0.14	0.30	0.48
Suburban/ Vertical	0.14	0.25	0.35
Suburban/ Circular	0.12	0.22	0.32
Urban/ Vertical	0.16	0.29	0.40
Urban High-Rise/ Vertical	0.57	0.91	1.10
Urban High-Rise/ Circular	0.56	0.87	1.13

6.2 Multipath Statistics

To fully characterize the multipath components for all APDPs in a given data set, a statistical description of signal amplitude variation for every delay time would be needed. One could show the cumulative distribution of signal amplitude for every delay time. A display of these results, however, would require a three-dimensional plot with delay time on the x axis, amplitude on the y axis, and probability of exceeding the y axis amplitude on the z axis. These plots would most likely be very difficult to read and interpret. Instead of presenting the data in a three-dimensional plot, statistics can be computed and presented as a series of two-dimensional plots. These statistics are used to show some of the information available from the cumulative distribution of signal amplitude for every delay time. These statistics form the multipath statistics presented in this report and include as a function of delay time: average multipath power, standard deviation of multipath power, peak multipath power, and probability of multipath power exceeding a threshold. Each of these types of statistics will be described in this section.

All of the multipath statistics, like the RMS delay spread statistics, are computed from the APDPs. The primary difference between computations such as RMS delay spread and these multipath statistics is that the RMS delay spread is computed for each APDP separately, then the statistics are developed. The amplitude relationship between the APDPs is not important in the computation of RMS delay spread. For computation of multipath statistics, however, the amplitude relationship between APDPs is important. Therefore, some type of amplitude normalization of the APDPs is required. Before computation of the multipath statistics, each APDP is normalized by amplitude shifting the entire APDP such that the peak sample in each APDP is set to 0 dB. This allows APDPs of varying total power to be treated on an equivalent basis for the computation of the multipath statistics.

The average multipath power shows the average power of a delayed signal at a given delay time for each data set listed in Table 6.1. Average multipath power as a function of delay time is computed as

$$P_{avg}(\tau_k) = \frac{\sum_{i=1}^{M} P_i(\tau_k)}{M}$$

where M is the total number of normalized APDPs for a given data set, τ_k is the time delay of the k^{th} sample in the APDP relative to the time of occurrence of the first perceptible reception of the transmitted signal (i.e., relative to time zero), and $P_i(\tau_k)$ is the value of the i^{th} APDP at a time delay of τ_k. The peak value in the plots of average multipath power *vs* delay time will usually be less than 0 dB. This is because the APDPs are aligned in time according to the first perceptible reception of the transmitted signal, not according to the peak sample in the APDP.

The standard deviation of multipath power shows the standard deviation of a delayed signal's power at a given delay time for each data set. The standard deviation of multipath power as a function of delay time is given as

$$P_{std}(\tau_k) = \left[\frac{\sum_{i=1}^{M} P_i^2(\tau_k)}{M} - P_{avg}^2(\tau_k) \right]^{\frac{1}{2}}$$

The peak multipath power shows the largest signal power that was observed at a given delay time for each data set. Peak multipath power is computed by finding the largest signal power at each delay time in all of the normalized APDPs for each data set.

The last type of multipath statistic is the probability of multipath power exceeding a threshold. For each data set, these statistics are computed by finding the probability that a delayed signal's power will be greater than a given threshold for each delay time. The computation is performed for each delay time by finding the number of normalized APDPs for a given data set in which the delayed signal power exceeds the threshold. This number is then divided by the total number of normalized APDPs for that data set. Four different threshold levels are used: -5 dB, -10 dB, -15 dB, and -20 dB where 0 dB represents the power of the peak sample in each normalized APDP.

Figures 6.7a-6.10a show average multipath power *vs* delay (solid line) and the associated standard deviation (broken line) for 915 MHz using vertically polarized transmit antennas for the semi-rural, suburban, urban, and urban high-rise cells, respectively. Figures 6.7b-6.10b show the same statistics for 1920 MHz. Essentially, there is little difference in the average multipath power between 915 MHz and 1920 MHz. As expected, the urban high-rise cell generates the largest average power for delays greater than 0.5 μs (Figures 6.10a-b). The results are almost identical for the semi-rural, suburban, and urban cells (Figures 6.7a-b, 6.8a-b, and 6.9a-b), however. It is of interest to note that the standard deviation curves tend to follow the average multipath power curves.

Plots of average multipath power and standard deviation of multipath power using circularly polarized transmit antennas can be seen in Figures 6.11a-b and 6.12a-b for the suburban, and urban high-rise cells respectively. In comparing these plots with the corresponding plots using vertically polarized transmit antennas (Figures 6.8a-b and 6.10a-b), certain trends can be noted which are consistent with the findings for RMS delay spread. In the suburban cell, for 1920 MHz, using the circularly polarized transmit antenna (Figure 6.11b), the average power is slightly lower (for delays greater than 0.5 μs) than when using the vertically polarized transmit antenna (Figure 6.8b). The same is true for delays greater than 1.5 μs in the urban high-rise cell (Figures 6.10a and 6.12a). Such differences, however, are not noticeable for 915 MHz. As pointed out earlier, these results suggest that the detrimental effects of multipath propagation may be reduced by using circular polarization in place of vertical polarization in the transmit antennas.

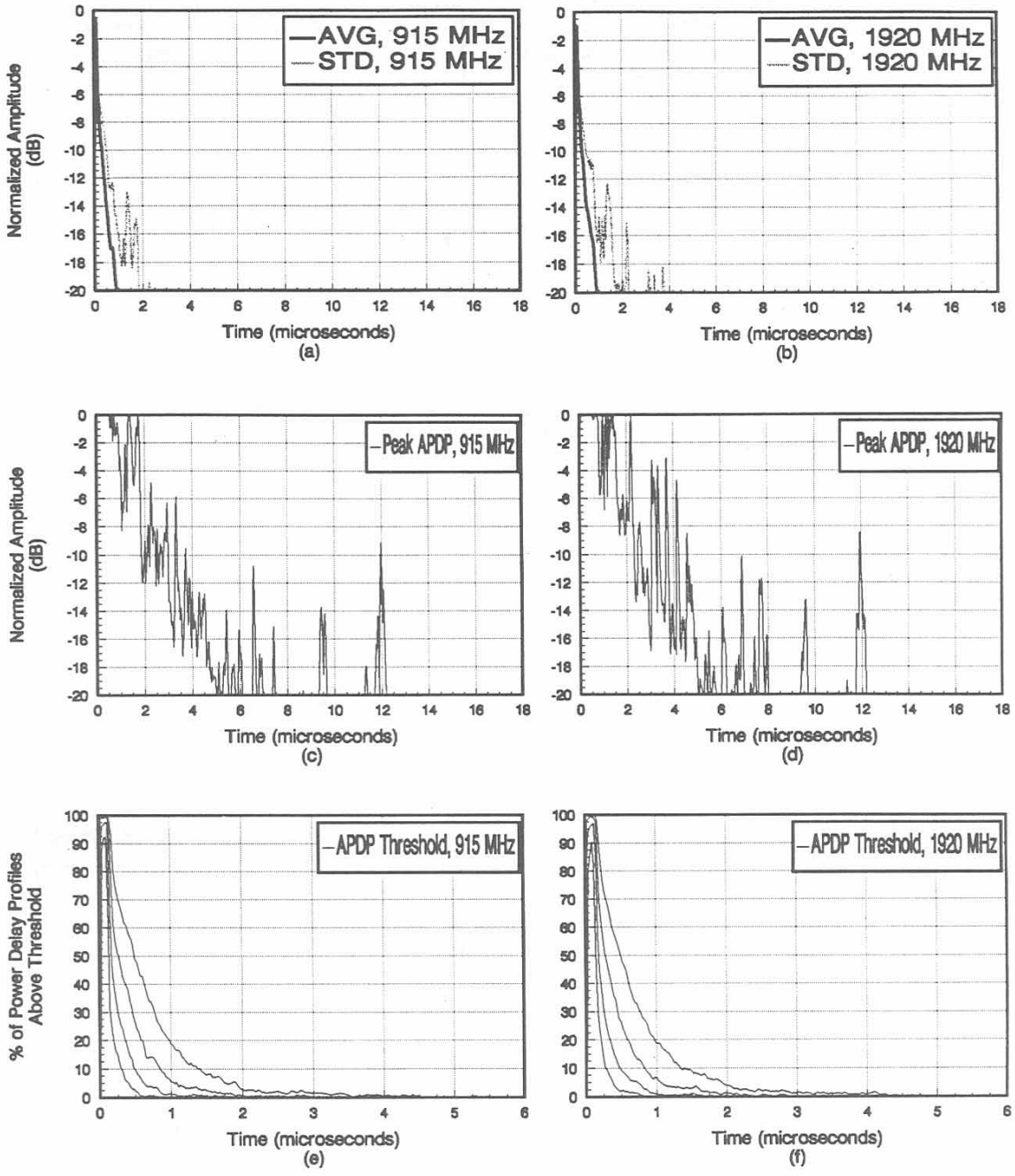

Figure 6.7. Multipath statistics for the semi-rural cell using vertically polarized transmit antennas.

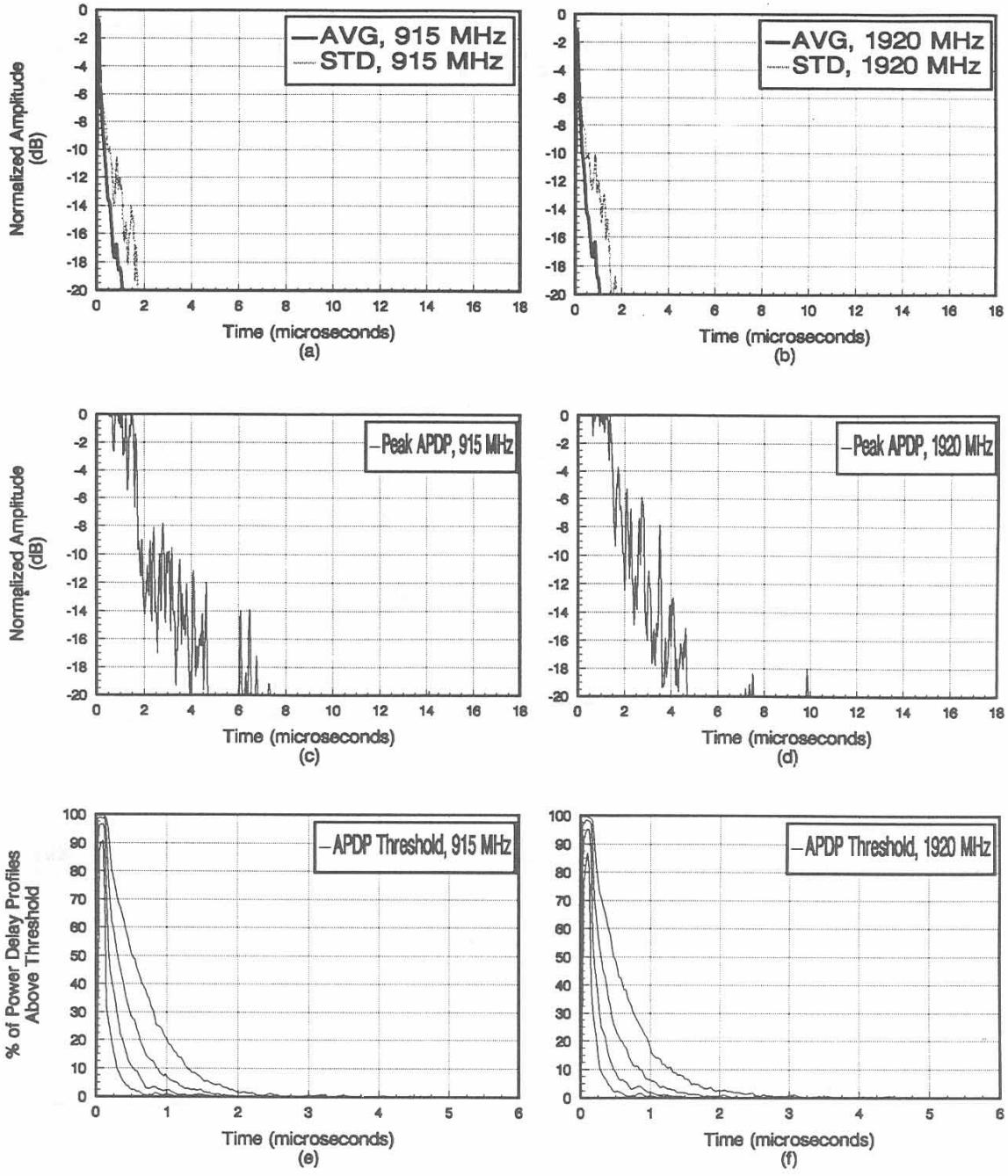

Figure 6.8. Multipath statistics for the suburban cell using vertically polarized transmit antennas.

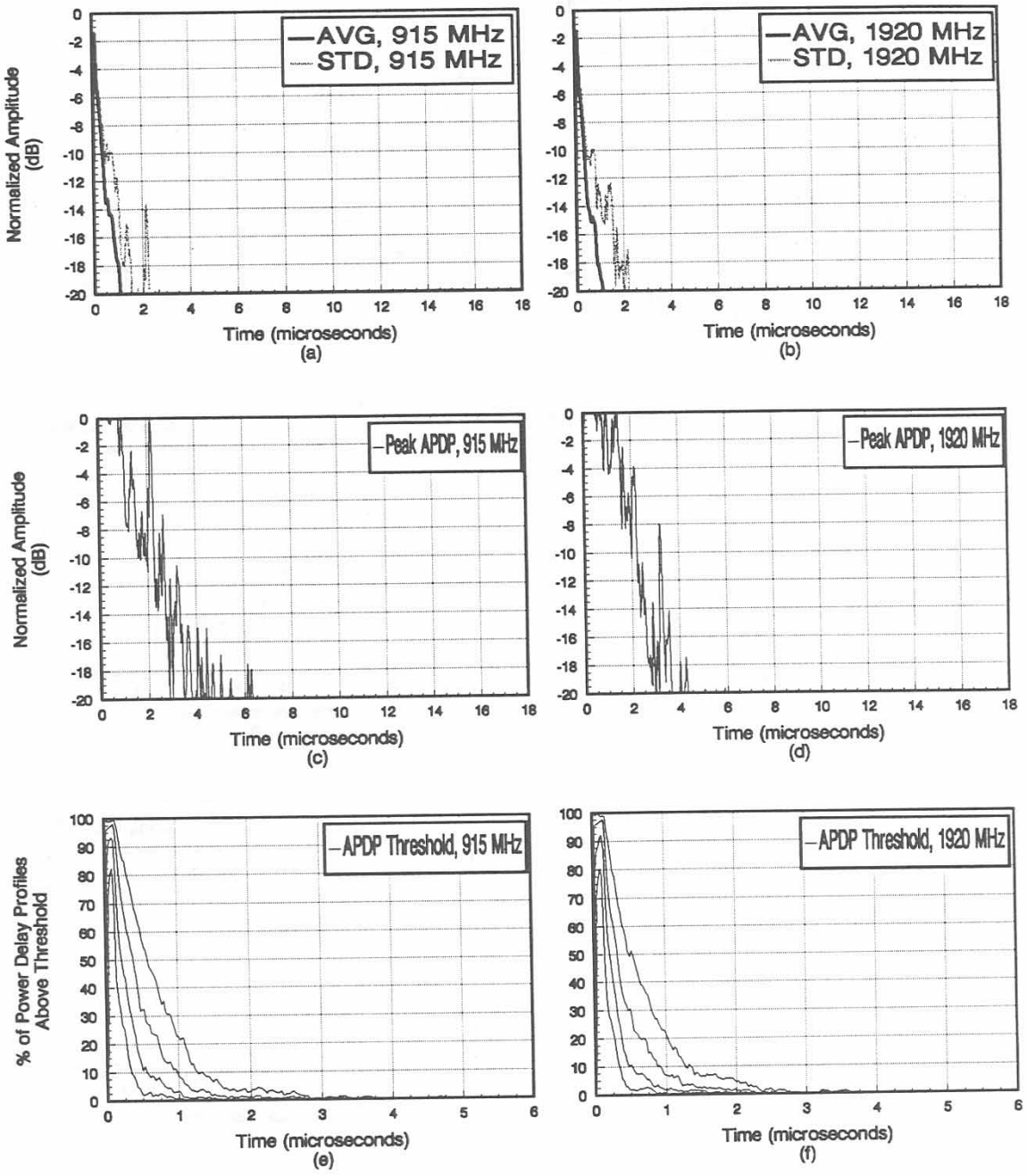

Figure 6.9. Multipath statistics for the urban cell using vertically polarized transmit antennas.

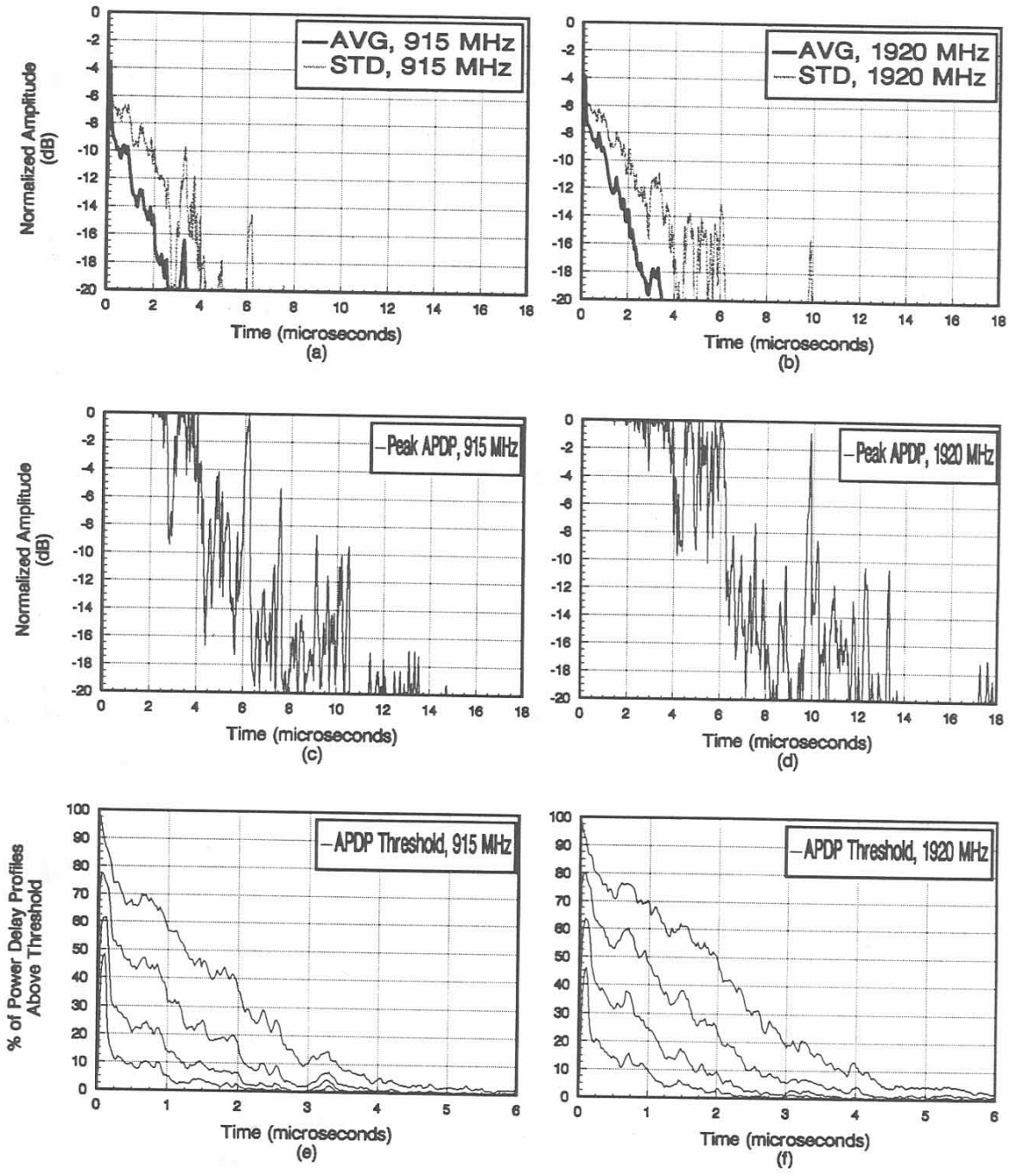

Figure 6.10. Multipath statistics for the urban high-rise cell using vertically polarized transmit antennas.

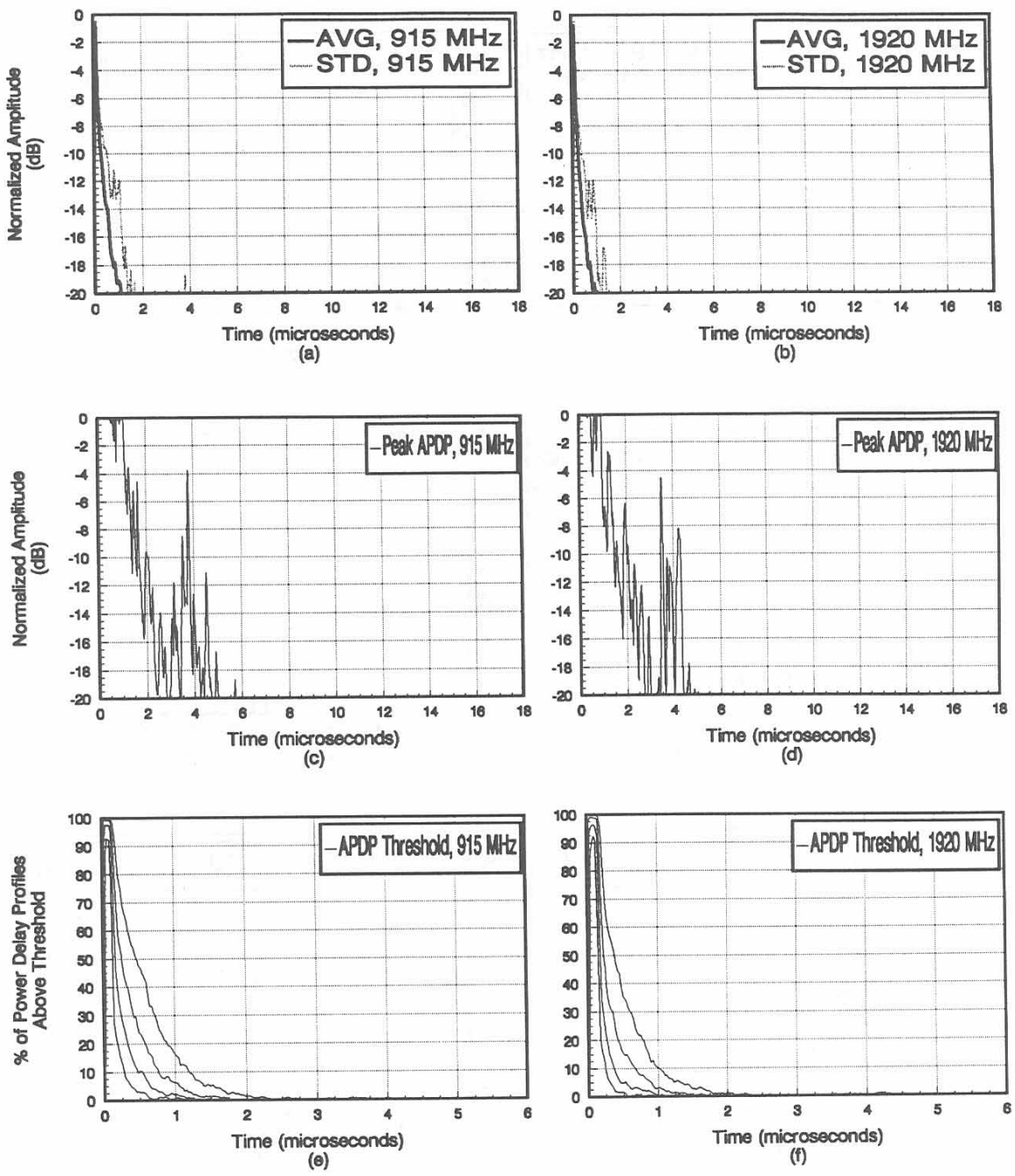

Figure 6.11. Multipath statistics for the suburban cell using circularly polarized transmit antennas.

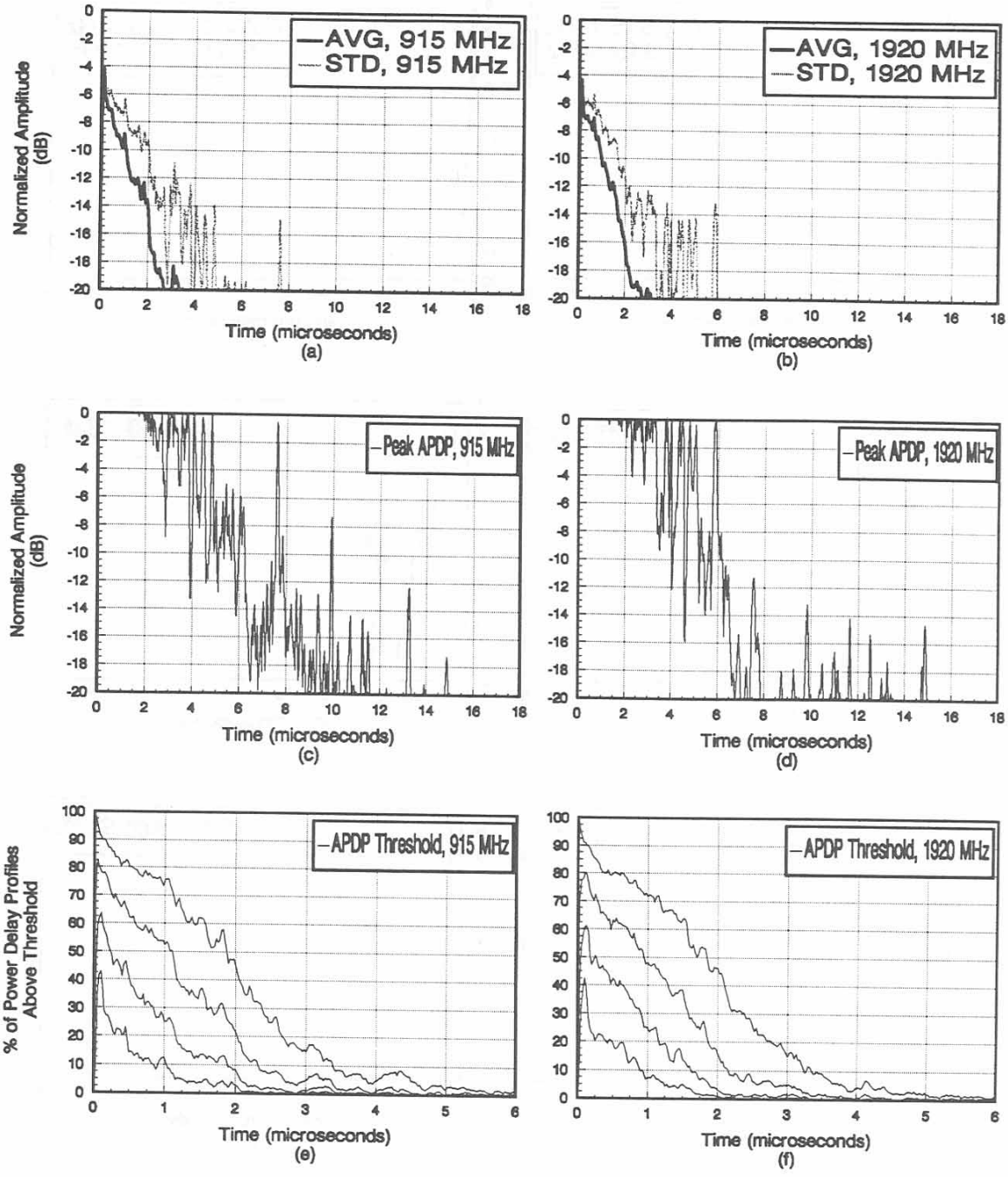

Figure 6.12. Multipath statistics for the urban high-rise cell using circularly polarized transmit antennas.

Figures 6.7c-6.10c show peak multipath power *vs* delay for 915 MHz using vertically polarized transmit antennas for the semi-rural, suburban, urban, and urban high-rise cells, respectively. Figures 6.7d-6.10d show the corresponding peak multipath power *vs* delay for 1920 MHz. The peak multipath power plots for both frequency bands appear somewhat similar. The greatest spread in peak multipath power with delayed signals up to 18 μs is seen for the urban high-rise cell (Figures 6.10c-d), as expected. As for RMS delay spread, the peak multipath power for the suburban and urban cells are very similar. However, the peak multipath power for the semi-rural cell (Figures 6.7c-d) is different from the suburban and urban cells in that it shows some moderately strong multipath delays up to 12 μs. This could account for the differences in RMS delay spread for the semi-rural cell as compared to the suburban and urban cells. Since the average multipath power does not show any corresponding multipath signals at these large delays, one could conclude that these large delays occur only occasionally. The probability of encountering these large multipath delays can be better seen in the threshold statistics described later in this section.

Peak multipath power using circularly polarized transmit antennas can be seen in Figures 6.11c-d and 6.12c-d for the suburban, and urban high-rise cells respectively. No specific patterns can be identified that show differences between these results and the corresponding results using the vertically polarized transmit antennas (Figures 6.8c-d and 6.10c-d).

Since each individual APDP is normalized so that the peak received multipath signal is set to 0 dB and since the first perceptible received copy of the signal is aligned to zero time, many of the values on the peak multipath plots up to 6 μs are 0 dB. This happens because the peak received multipath signal frequently occurs some time after the first perceptible received signal. This occurs when a received copy of the signal with the greatest power follows a route between the transmitter and receiver that is longer than the first received signal (as is often the case during non line-of-sight transmitter/receiver orientation). In the graphs of average multipath power *vs* delay, the amplitude normalization and time alignment result in having all points on the graph lie somewhere below 0 dB.

Figures 6.7e-6.10e show the probability of multipath power exceeding four different thresholds for 915 MHz using vertically polarized transmit antennas for the semi-rural, suburban, urban, and urban high-rise cells, respectively. Figures 6.7f-6.10f show the corresponding threshold statistics for 1920 MHz. For each graph, the top curve represents the probability of the normalized multipath power exceeding -20 dB. The second, third, and fourth curves from the top represent the probability of the normalized multipath power exceeding -15 dB, -10 dB, and -5 dB respectively. For example, in Figure 6.10e we see that for a delay of 1.0 μs, there is a 5% chance that the normalized multipath signal will exceed -5 dB. In addition, there is a 14% chance of exceeding -10 dB, a 31 % chance of exceeding -15 dB, and a 57 % chance of exceeding -20 dB.

There is very little difference between the threshold statistics for the semi-rural, suburban and urban cells (Figures 6.7e-f, 6.8e-f, and 6.9e-f). For the urban high-rise cell (Figures 6.10e-f), there are considerably higher percentages of APDPs above threshold for all thresholds than

in the other cells (for delays greater than 0.5 μs). In addition, the differences between 915 MHz and 1920 MHz are negligible for the semi-rural, suburban, and urban cells. For the urban high-rise cell, however, there are higher percentages of APDPs above threshold for 1920 MHz for all thresholds than for 915 MHz (for delays greater than 0.25 μs).

Threshold statistics using circularly polarized transmit antennas can be seen in Figures 6.11e-f and 6.12e-f for the suburban and urban high-rise cells respectively. There are some differences between these plots and the corresponding plots using vertically polarized transmit antennas (Figures 6.8e-f and 6.10e-f). No consistent pattern characterizing these differences can be established, though.

6.3 Correlation Bandwidth

The correlation bandwidth (sometimes called coherence bandwidth) is the bandwidth in which the spectral components of the transmitted signal are affected in a similar way (Macario, 1991). In order to find the correlation bandwidth, the autocorrelation of the frequency transfer function of the channel must be determined. An easy way to obtain this autocorrelation is by taking the Fourier transform of $|h(t)|^2$, the magnitude squared of the complex impulse response of the channel (CCIR, 1990). Since the APDPs are digitized bandlimited approximations to $|h(t)|^2$, they may be used to obtain approximations to the autocorrelation of the frequency transfer function.

The procedure to compute correlation bandwidth therefore begins by taking the discrete Fourier transform of each APDP. The magnitude of this quantity is given as $|G(jf_k)|$ and represents an approximation to the magnitude of the autocorrelation of the frequency transfer function of the channel. Note that f_k is the frequency of the k^{th} point along the spectrum and ranges from 0 to 20 MHz. The discrete Fourier transform is then taken of a PDP generated from the measurement system with the transmitter and receiver connected back-to-back. The magnitude of this quantity is given as $|F(jf_k)|$. The effects of the measurement system are removed by dividing $|G(jf_k)|$ by $|F(jf_k)|$ (Cox and Leek, 1975). The resulting magnitude spectrum is then used to determine the 90% and 50% correlation bandwidths ($Bc_{0.9}$ and $Bc_{0.5}$) by finding the frequencies at which the magnitude is 90% and 50% of the peak value, respectively. For each of the 12 data sets listed in Table 6.1, the probability density and cumulative distribution of $Bc_{0.9}$ and $Bc_{0.5}$ are then computed.

Figures 6.13a-6.16a show the probability densities of the 50% correlation bandwidth $Bc_{0.5}$ for 915 MHz using vertically polarized transmit antennas for the semi-rural, suburban, urban, and urban high-rise cells, respectively. Figures 6.13b-6.16b show the corresponding statistics for 1920 MHz. The probability density functions shown here are approximate and are determined from histograms with 19.6-kHz bins. Values on each of these plots represent the percentage of APDPs for a given data set having a $Bc_{0.5}$ that falls within a particular 19.6-kHz bin. In the semi-rural, suburban, and urban cells, the probability densities of $Bc_{0.5}$ show a fairly even distribution over all frequencies up to 18 MHz. For the urban high-rise cell, the

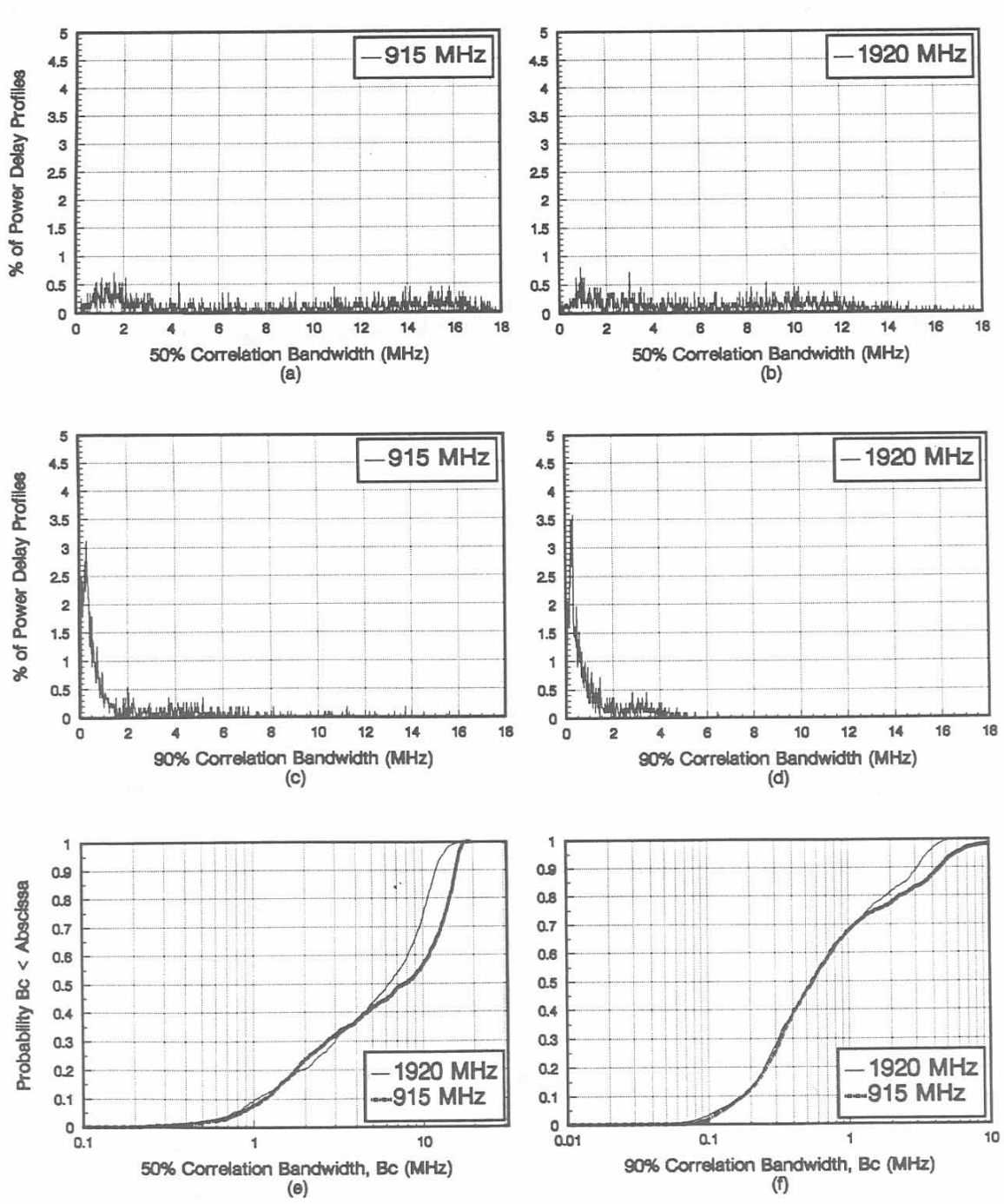

Figure 6.13. Probability density (a-d) and cumulative distribution (e-f) of correlation bandwidth for the semi-rural cell using vertically polarized transmit antennas.

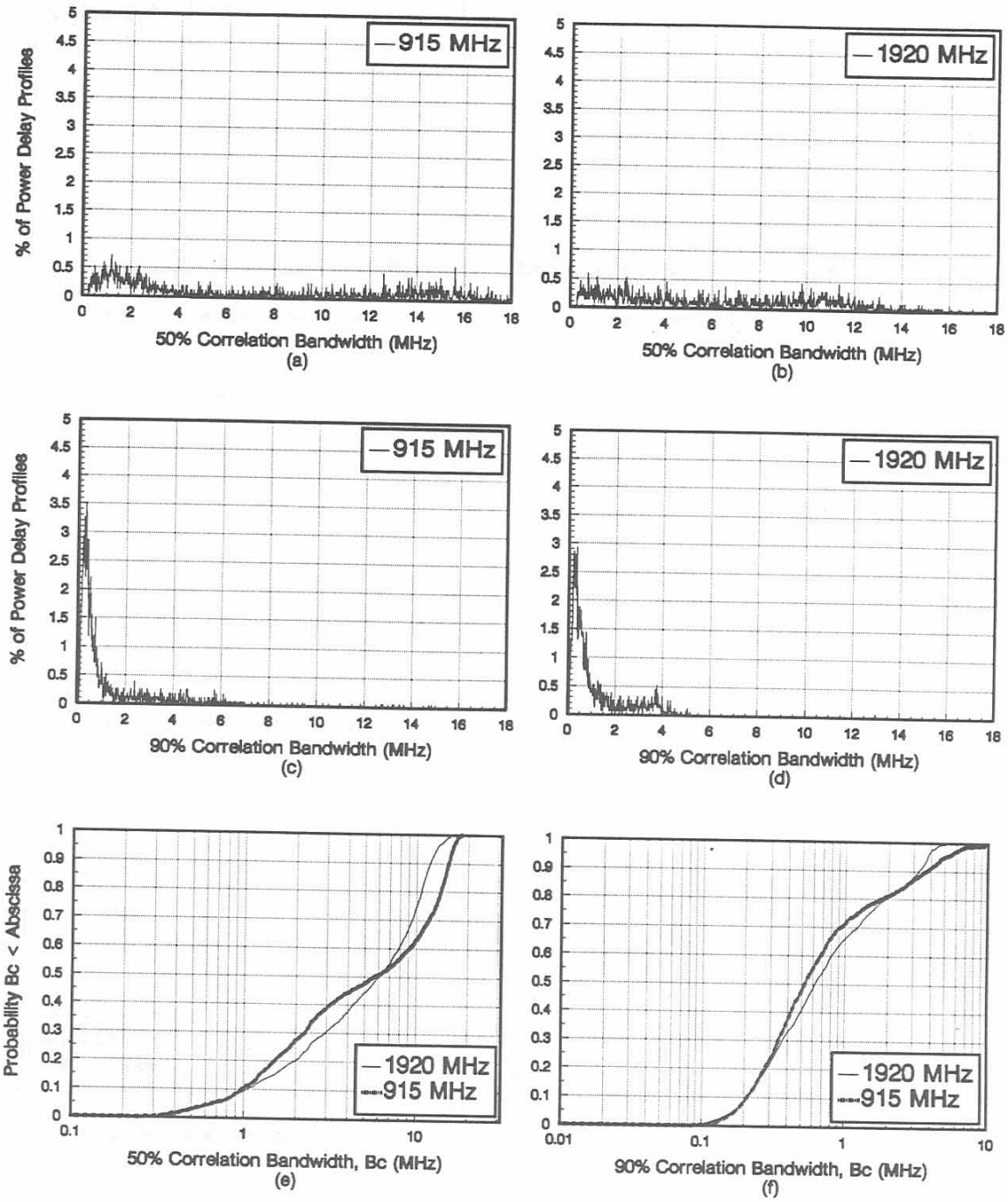

Figure 6.14. Probability density (a-d) and cumulative distribution (e-f) of correlation bandwidth for the suburban cell using vertically polarized transmit antennas.

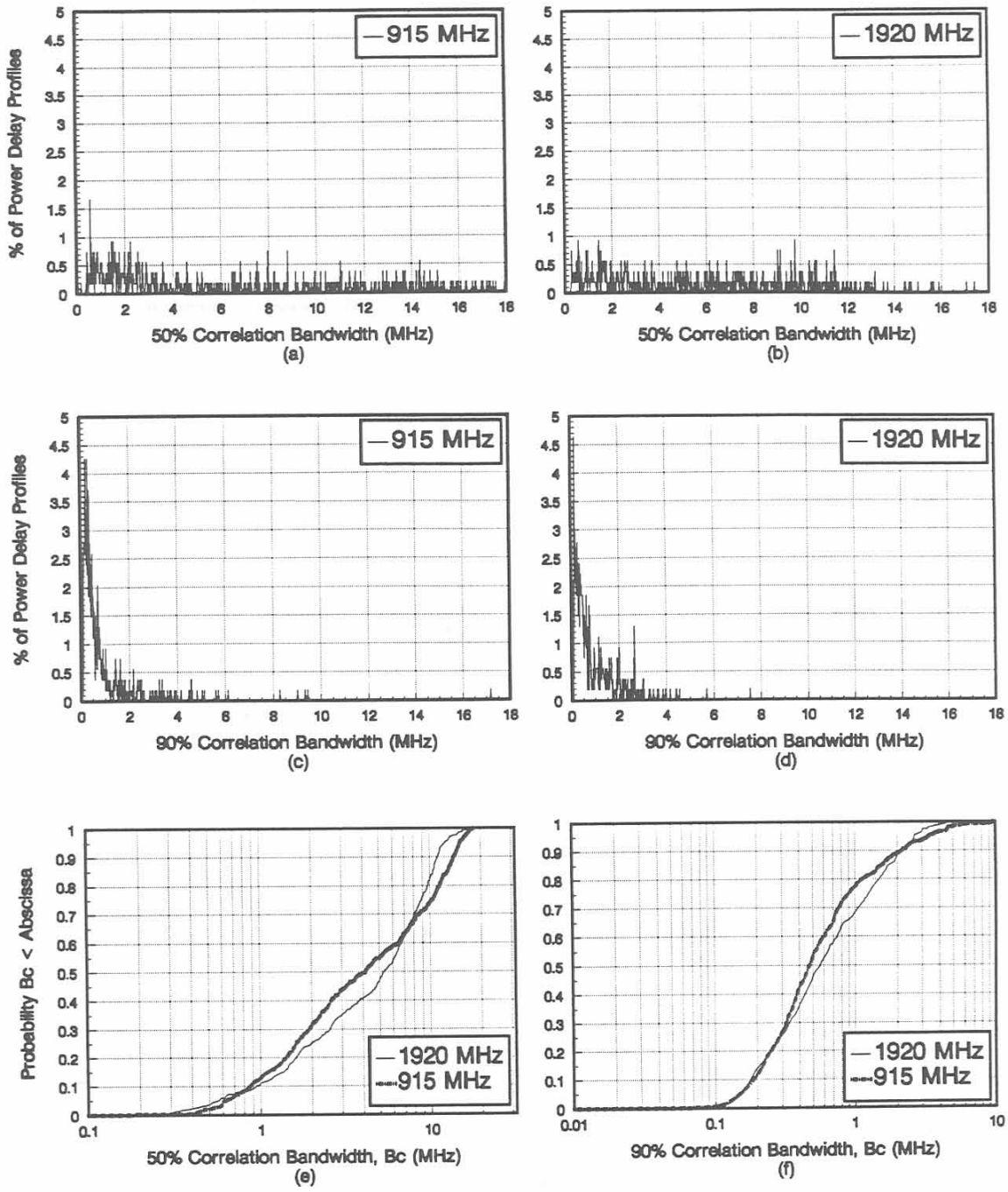

Figure 6.15. Probability density (a-d) and cumulative distribution (e-f) of correlation bandwidth for the urban cell using vertically polarized transmit antennas.

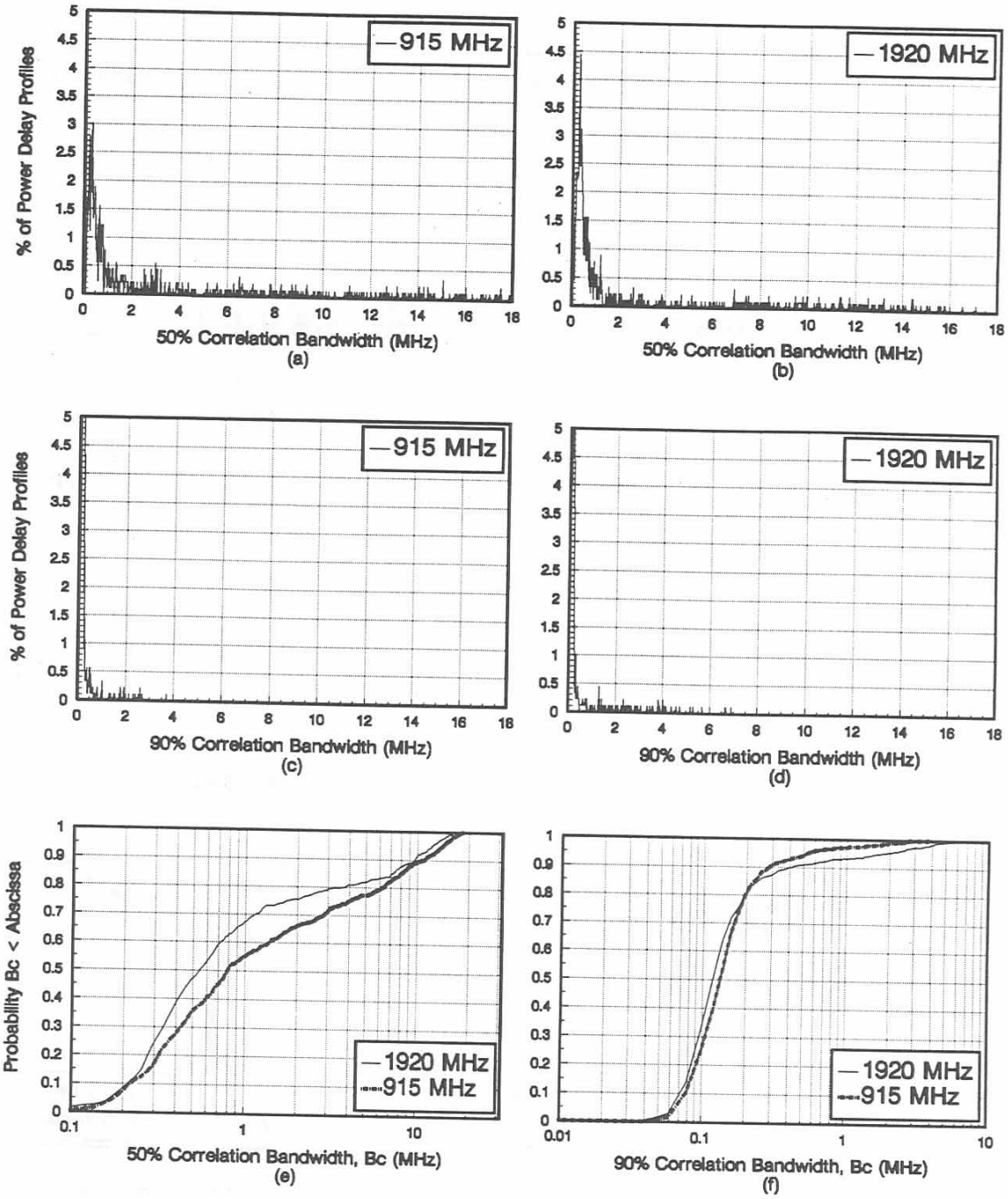

Figure 6.16. Probability density (a-d) and cumulative distribution (e-f) of correlation bandwidth for the urban high-rise cell using vertically polarized transmit antennas.

probability density shows that values of $Bc_{0.5}$ approximately 1.0 MHz or less occur most frequently.

Figures 6.13e-6.16e show the cumulative distributions of $Bc_{0.5}$ for each of the cells using the vertically polarized transmit antennas. Statistics for both 915 MHz and 1920 MHz are plotted on the same graph to facilitate the comparison of propagation between the two bands. Values on each plot represent the probability that $Bc_{0.5}$ is less than the corresponding frequency on the abscissa. For example, Figure 6.15e shows a probability of 0.1 that $Bc_{0.5}$ is less than 1 MHz for 1920 MHz and a probability of 0.1 that $Bc_{0.5}$ is less than 0.87 MHz for 915 MHz. There is a small difference in the cumulative distribution of $Bc_{0.5}$ between 1920 MHz and 915 MHz for the semi-rural, suburban, and urban cells using the vertically polarized transmit antennas. This difference is more pronounced in the urban high-rise cell. Cumulative distribution curves of $Bc_{0.5}$ for the semi-rural, suburban, and urban cells are all fairly similar. The urban high-rise cell shows the greatest probability for $Bc_{0.5}$ to be less than the abscissa as compared to the other cell types. This was an expected result since more multipath is expected in this cell and more multipath typically implies a smaller correlation bandwidth.

Figures 6.13c-d through 6.16c-d show the probability densities of the 90% correlation bandwidth $Bc_{0.9}$ for each of the cells using the vertically polarized transmit antennas. Figures 6.13f-6.16f represent the cumulative distribution of $Bc_{0.9}$ for each of the cells using the vertically polarized transmit antennas. The cumulative distribution curves for $Bc_{0.9}$ show the same sort of trends as seen for $Bc_{0.5}$ except that the differences in the curves between 915 and 1920 MHz are smaller. These differences are also no more pronounced in the urban high-rise cell than in the other cells.

Correlation bandwidth statistics using circularly polarized transmit antennas can be seen in Figures 6.17a-f and 6.18a-f for the suburban and urban high-rise cells respectively. While comparisons between the $Bc_{0.5}$ cumulative distribution curves using vertically and circularly polarized transmit antennas do not yield any conclusive results, those between the corresponding $Bc_{0.9}$ curves do. Compare the cumulative distribution curves for $Bc_{0.9}$ (Figures 6.17f and 6.18f) with the corresponding curves using vertically polarized transmit antennas (Figures 6.14f and 6.16f). For 1920 MHz, the cumulative distributions of $Bc_{0.9}$ using the vertically polarized transmit antennas show a greater probability for $Bc_{0.9}$ to be less than the abscissa than the corresponding statistics using circularly polarized transmit antennas. This phenomenon is also seen in the suburban cell for 915 MHz. Considering error bounds, however, there may be no real difference in the population cumulative distributions of $Bc_{0.9}$ using vertically or circularly polarized transmit antennas for 915 MHz. For 1920 MHz, the $Bc_{0.9}$ results suggest that the detrimental effects of multipath propagation may be reduced by using circular polarization in the transmit antennas. This same conclusion was reached from the RMS delay spread statistics.

Tables 6.5 and 6.6 provide for a quantitative comparison of the cumulative distributions of $Bc_{0.5}$ between the various cells and between both transmit antenna polarizations for 1920 MHz and 915 MHz respectively. These tables show values of $Bc_{0.5}$ (in MHz) for which there is a fixed probability of not exceeding. For example, for 1920 MHz, there is a probability of 0.1 that $Bc_{0.5}$ will be less than 0.21 MHz in the urban high-rise cell using vertical polarization. On the other hand, for 1920 MHz, there is a probability of 0.1 that $Bc_{0.5}$ will be less than 0.93 MHz in the urban cell using vertical polarization.

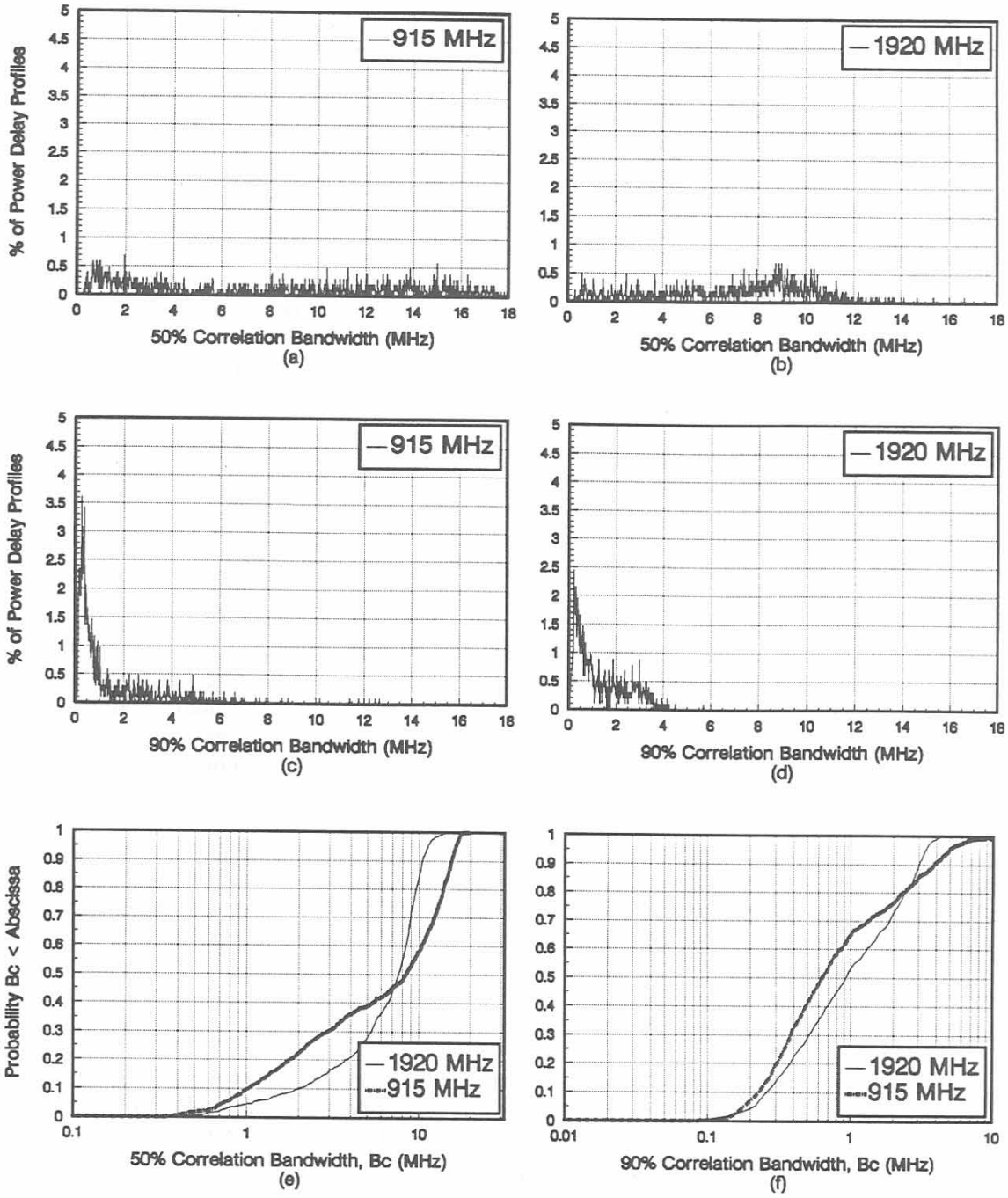

Figure 6.17. Probability density (a-d) and cumulative distribution (e-f) of correlation bandwidth for the suburban cell using circularly polarized transmit antennas.

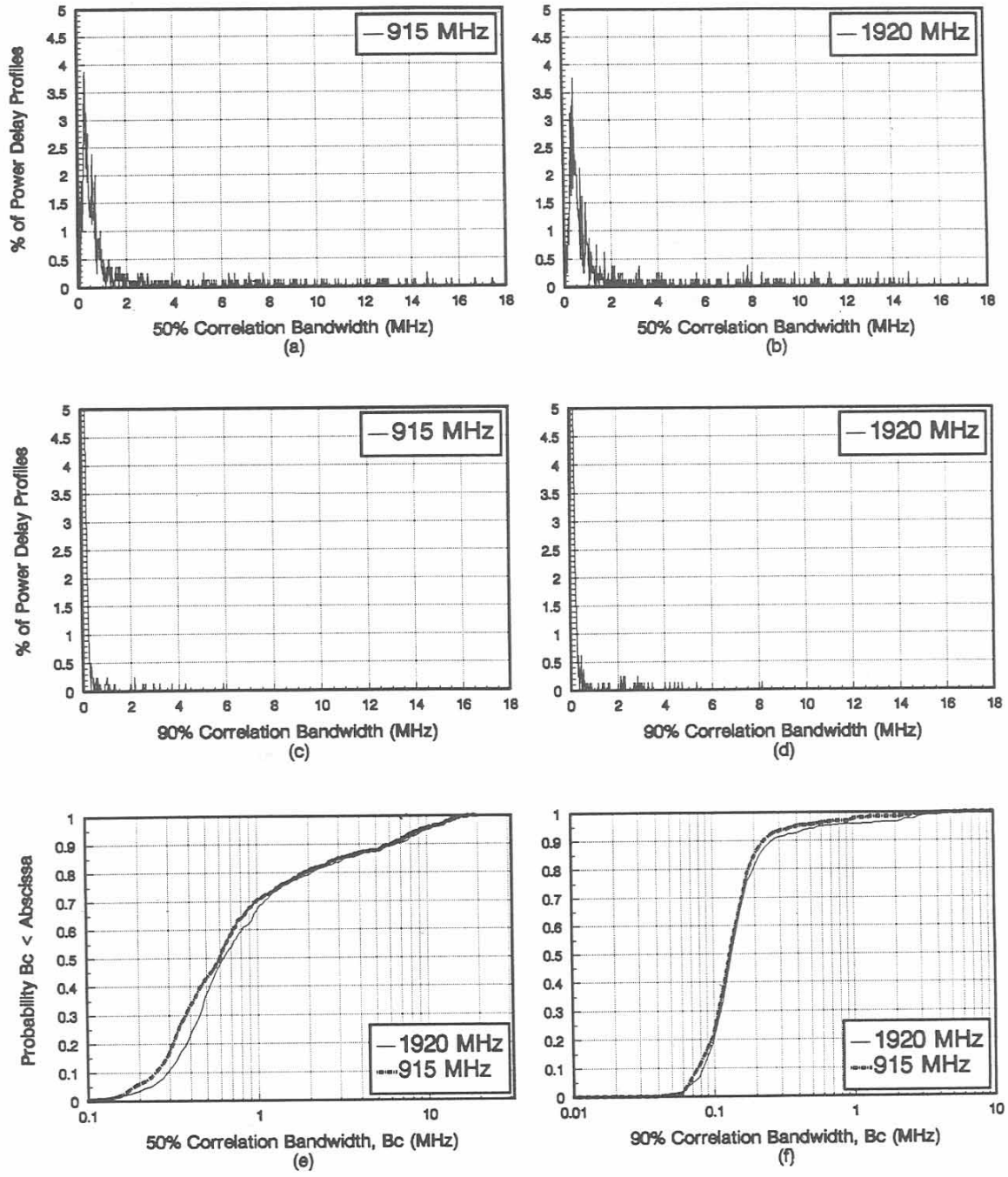

Figure 6.18. Probability density (a-d) and cumulative distribution (e-f) of correlation bandwidth for the urban high-rise cell using circularly polarized transmit antennas.

Table 6.5. Comparison of 50% Correlation Bandwidth Values Not Exceeded (in MHz) for 1920 MHz

Cell Type/Antenna Polarization	Probability of being less than $Bc_{0.5}$		
	0.5	0.2	0.1
Semi-Rural/ Vertical	6.22	1.89	1.03
Suburban/ Vertical	6.04	1.92	1.05
Suburban/ Circular	7.59	3.69	1.98
Urban/ Vertical	5.27	1.61	0.93
Urban High-Rise/ Vertical	0.54	0.28	0.21
Urban High-Rise/ Circular	0.63	0.38	0.29

Table 6.6. Comparison of 50% Correlation Bandwidth Values Not Exceeded (in MHz) for 915 MHz

Cell Type/Antenna Polarization	Probability of being less than $Bc_{0.5}$		
	0.5	0.2	0.1
Semi-Rural/ Vertical	7.69	1.75	1.14
Suburban/ Vertical	5.64	1.50	0.97
Suburban/ Circular	8.39	1.77	1.02
Urban/ Vertical	4.13	1.41	0.86
Urban High-Rise/ Vertical	0.79	0.32	0.22
Urban High-Rise/ Circular	0.60	0.31	0.25

7. SUMMARY AND CONCLUSIONS

This report discusses a PCS propagation experiment to conduct impulse response measurements in the 902-928 and 1850-1990 MHz bands simultaneously. The measurements were taken in four different macrocells (with radii ranging from 3 to 11 km) in the Philadelphia, PA area. The cells were chosen to represent typical semi-rural, suburban, urban, and urban high-rise environments. Measurements were taken in all four cells using vertically polarized transmit and receive antennas. In the suburban and urban high-rise cells, measurements were also taken using circularly polarized transmit antennas (the receive antennas were vertically polarized).

The impulse response measurement system consisted of a transmitter placed at existing cellular base station sites and a receiver located in a measurement van. A GPS receiver and dead-reckoning system were employed to store time and vehicle position information for the measurement van. A description of the measurement system was given. Several different types of calibration and system verification procedures were performed to ensure optimal system operation. These procedures included reference oscillator locking between the transmitter and receiver, amplitude calibration, antenna and feed cable testing, and an over-the-air system check. The measurement and data collection process followed for all of the measurements was discussed in detail. Impulse response data were recorded as the measurement van travelled along predetermined routes within each cell. The routes were chosen to provide a representative characterization of the propagation behavior in each cell. Data were recorded simultaneously in both the 902-928 and 1850-1990 MHz bands. Three different acquisition schemes were used to take the data. Only data taken using the fast acquisition scheme were used for analysis in this report. In this scheme, every 0.5 s, a rapid succession of three impulse responses was taken. Within this succession of impulses, a time interval of 1.5 ms was used between the start of one impulse and the start of another. The data collected in this manner ensured that the Doppler shift could be determined; an important factor for analyses such as angle-of-arrival. Vehicle velocity was limited to 50 mph or less (for the fast acquisition scheme) and varied depending on the particular measurement route.

The impulse response data were analyzed to provide RMS delay spread, correlation bandwidth, and various other multipath power statistics. The results of this data analysis provided a comparison of wideband propagation between the two frequency bands, the two transmit antenna polarizations, and between the different cell types. Major differences in the propagation behavior between the two frequency bands were not seen. The urban high-rise cell exhibited the most multipath, showing higher power and more delayed signals with longer delays than in the other cells. Propagation behavior in the suburban and urban cells was very similar. The semi-rural cell, however, displayed more multipath than the suburban and urban cells, probably due to hilly terrain (in the semi-rural cell). An improvement in propagation (less multipath) was seen when using the circularly polarized transmit antennas instead of the vertically polarized ones for 1920 MHz. This trend was not apparent for 915 MHz. These results suggest that the detrimental effects of multipath propagation may be reduced by using

circular polarization in place of vertical polarization in the transmit antennas of a PCS system operating in various macrocellular environments. Additionally, the results suggest that these benefits obtained by changing the transmit antenna polarization may be more significant for 1920 MHz than for 915 MHz. Further polarization studies are recommended to investigate these possible benefits.

8. REFERENCES

CCIR (1990), Propagation data and prediction methods for the terrestrial land mobile service using the frequency range 30 MHz to 3 GHz, CCIR Report 567-4, International Radio Consultive Committee, International Telecommunications Union, Geneva, Switzerland.

Cox, D.C. (1972a), Delay Doppler characteristics of multipath propagation at 910 MHz in a suburban mobile radio environment, *IEEE Trans. on Antennas and Propagation,* AP-20, No.5, September, pp. 625-635.

Cox, D.C. (1972b), Time- and frequency-domain characterizations of multipath propagation at 910 MHz in a suburban mobile-radio environment, *Radio Science,* Vol. 7, No. 12, December, pp. 1069-1077.

Cox, D.C., and R.P. Leek (1975), Correlation bandwidth and delay spread multipath propagation statistics for 910 MHz urban mobile radio channels, *IEEE Trans. on Communications,* COM-23, No. 11, November, pp. 1271-1280.

Devasirvatham, D.M.J. (1987), Multipath time delay spread in the digital portable radio environment, *IEEE Communications Magazine,* Vol. 25, No.6, June, pp. 13-21.

Dixon, W.J. and Massey, F.J. (1969), *Introduction to Statistical Analysis,* (McGraw-Hill, Inc., New York), pp. 345-347.

Macario, R.C.V (1991), *Personal and Mobile Radio Systems* (Peter Peregrinus, Ltd., London, U.K.), pp. 31-32.

Tanis, W.J. II (1993), Bell Atlantic Mobile Systems PCS Propagation Research: Fifth Quarterly Report to the FCC, Experimental License Report for Station KI2XFO, File No. 1900-EX-PL-91, February 2, 1993, pp. 40-48.

ACKNOWLEDGMENTS

The authors would like to thank William J. Tanis II and Michael E. Hughes of Bell Atlantic Mobile, Inc. for their many contributions during all phases of this work. Without the assistance of these individuals, this work would not have been possible.

FORM **NTIA-29**
(4-80)

U.S. DEPARTMENT OF COMMERCE
NAT'L. TELECOMMUNICATIONS AND INFORMATION ADMINISTRATION

BIBLIOGRAPHIC DATA SHEET

	1. PUBLICATION NO.	2. Gov't Accession No.	3. Recipient's Accession No.
	93-299		

4. TITLE AND SUBTITLE
Comparison of Wideband Propagation in the 902-928 and 1850-1990 MHz Bands in Various Macrocellular Environments

5. Publication Date
September, 1993

6. Performing Organization Code
NTIA/ITS

7. AUTHOR(S)

9. Project/Task/Work Unit No.

8. PERFORMING ORGANIZATION NAME AND ADDRESS
NTIA/ITS
325 Broadway
Boulder, CO. 80303

10. Contract/Grant No.

11. Sponsoring Organization Name and Address
Bell Atlantic Mobile, Inc.
180 Washington Valley Road
Bedminster, NJ 07921

12. Type of Report and Period Covered

13.

14. SUPPLEMENTARY NOTES

15. ABSTRACT *(A 200-word or less factual summary of most significant information. If document includes a significant bibliography or literature survey, mention it here.)*

Impulse response measurements were taken simultaneously in both the 902-928 and 1850-1990 MHz bands using a wideband measurement system consisting of a fixed transmitter and a mobile receiver. Four different macrocells representing typical semi-rural, suburban, urban, and urban high-rise environments were used for the measurements. Vertically polarized transmit and receive antennas were used for all cells; circularly polarized transmit antennas were also used in the suburban and urban high-rise cells. RMS delay spread, correlation bandwidth, and various other multipath power statistics were used to characterize the wideband propagation and to provide a comparison between the two frequency bands, the two transmit antenna polarizations, and the different cell environments. Major differences were not seen in the propagation behavior between the two frequency bands. The urban high-rise cell exhibited the most multipath, showing more delayed signals having higher power and longer delays than in the other cells. An improvement in propagation (less multipath) was seen when using the circularly polarized transmit antennas instead of the vertically polarized ones for 1920 MHz.

16. Key Words *(Alphabetical order, separated by semicolons)*

Coherence bandwidth; correlation bandwidth; impulse response measurements; PCS; Personal Communications Services; power delay profiles; RMS delay spread; wideband measurements.

17. AVAILABILITY STATEMENT

☒ UNLIMITED.

☐ FOR OFFICIAL DISTRIBUTION.

18. Security Class. *(This report)*

20. Number of pages

19. Security Class. *(This page)*

21. Price:

☆ U.S. Government Printing Office: 1980—678-495/529